Mendis, B.G. and MacKenzie, M. and Craven, A.J. (2010) *A new analytical method for characterising the bonding environment at rough interfaces in high-k gate stacks using electron energy loss spectroscopy*. Ultramicroscopy, 110 (2). pp. 105-117. ISSN 0304-3991

http://eprints.gla.ac.uk/32590/

Deposited on: 13 July 2010

Enlighten – Research publications by members of the University of Glasgow
http://eprints.gla.ac.uk

A new analytical method for characterising the bonding environment at rough interfaces in high- *k* gate stacks using electron energy loss spectroscopy

B. G. Mendis [a,b] [*] [†], **M. MacKenzie** [a] **and A. J. Craven** [a,b]

a *Dept. of Physics and Astronomy, University of Glasgow, Glasgow, G12 8QQ, UK*
b *SuperSTEM, Daresbury Laboratory, Keckwick Lane, Daresbury, WA4 4AD, UK*

[*] Now at Dept. of Physics, Durham University, Durham, DH1 3LE, UK.
[†] Corresponding author: b.g.mendis@durham.ac.uk

Abstract

Determining the bonding environment at a rough interface, using for example the near edge fine structure in electron energy loss spectroscopy (EELS), is problematic since the measurement contains information from the interface and surrounding matrix phase. Here we present a novel analytical method for determining the interfacial EELS difference spectrum (with respect to the matrix phase) from a rough interface of unknown geometry which, unlike multiple linear least squares (MLLS) fitting, does not require the use of reference spectra from suitable standards. The method is based on analysing a series of EELS spectra with variable interface to matrix volume fraction and, as an example, is applied to a TiN/ poly-Si interface containing oxygen in a HfO_2- based, high- *k* dielectric gate stack. A silicon oxynitride layer was detected at the interface consistent with previous results based on MLLS fitting.

1. Introduction

Many technologically important multilayer thin films, such as high- *k* dielectric gate stacks, contain rough interfaces. This paper is concerned with hafnia based dielectrics such as HfO_2 and HfSiO where the latter is a co-deposition of HfO_2 and SiO_2. Interface roughening can be caused by crystallisation, phase separation, interdiffusion, chemical reaction or may be due to a columnar grain structure. Electron energy loss spectroscopy (EELS) and energy dispersive X-ray (EDX) spectroscopy in a scanning transmission electron microscope (STEM) have been used previously to characterise the microstructure of high- *k* gate stacks, particularly at the interfaces [1-7]. For dielectrics involving Hf-Si-O with poly-Si gate electrodes, a silica (SiO_2)- type layer has been observed at the dielectric/ gate electrode interface [1,3,5]. When a TiN metal gate is used in combination with HfO_2 or HfSiO, the interface between TiN and the subsequent poly-Si electrode showed a silicon oxynitride (SiO_xN_y) interface layer [3,6-7]. However, a HfSiO dielectric with a TaN_x gate showed only a SiO_2 interface layer [8]. Such interfacial layers in series with the gate oxide are deleterious to device performance since by decreasing the overall dielectric constant the equivalent oxide thickness is increased.

The near edge fine structure (i.e. ELNES) of core loss edges in electron energy loss spectroscopy is governed by the bonding environment of the ionised atom and is a powerful tool for characterising thin interfacial layers. To a first approximation, the EELS spectrum that is acquired from a rough interface will be a mixture of the interfacial layer as well as the overlapping matrix phase(s) and can therefore be modeled as a linear combination of suitably chosen reference EELS spectra using multiple linear least squares (MLLS) fitting. As an example MacKenzie *et al.* [6] have used MLLS fitting to show the presence of a SiO_xN_y interfacial layer at the interface between TiN and poly-Si gate electrodes in a HfO_2- based dielectric gate stack. The Si- $L_{2,3}$ EELS spectrum acquired from the TiN/ poly-Si interface was MLLS fitted with Si- $L_{2,3}$ reference spectra from bulk Si, SiO_x and SiN_y [6]. The reference spectrum for bulk Si took into account the signal from the overlapping poly-Si matrix while the SiO_x and SiN_y spectra were used to model interfacial SiO_xN_y bonding. Similarly the N- K edge at the interface was successfully modeled using reference spectra from the bulk TiN matrix phase as well as SiN_y (the latter represents nitrogen bonding in the SiO_xN_y interfacial layer). There must also be a component from the interface itself where the modified environments change the ELNES but this is more difficult to detect and requires an excellent signal-to-noise ratio in the data. MacKenzie *et al*. detected changes in the N- K edge ELNES at the HfO_2/ TiN interface but it remains unclear whether this is simply the change of environment at the interface or an actual reaction layer [6].

Despite the success of MLLS fitting there are still several disadvantages. These include determining *a posteriori* suitable reference spectra. In many cases, it may be difficult to acquire reference spectra under the same experimental conditions used for interface analysis. Furthermore the interfacial spectrum may be different from that of the bulk despite there being no chemical reaction or interdiffusion taking place. For example, at the Si/ SiO_2 interface extra intensity below the edge onset of the O- K and Si- $L_{2,3}$ edges is observed due to interfacial states within the band gap [9-10]. Hence errors in MLLS fitting can arise if the ‘ideal’ interface is not included as a reference spectrum [2]. It is therefore desirable to use an analytical method that decouples the true interfacial EELS spectrum from the overlapping matrix signal in a rough interface without the use of standards. In this paper such a technique is presented and is based on a method developed by Rečnik and co-workers [11-14] for measuring segregation to planar boundaries. The concentration of Sn at a ZnO inversion boundary was measured using electron probes of different diameters; the larger the probe diameter the greater the contribution of the surrounding matrix so that the measurement is less sensitive to segregation at the inversion boundary. The variation of the measured composition as a function of probe diameter is used to obtain a more accurate measure of the segregation. As suggested in [14] by scanning the electron probe in a STEM, EELS spectra can be acquired over a region large enough to contain the interface as well as bulk matrix. Analysis regions with a large matrix volume are less sensitive to ELNES changes at the interface. Hence, by varying the interface to matrix volume fraction within the analysis region, the true interfacial bonding can be determined independently of any external standards. It is worth mentioning that the method of Rečnik and co-workers [11-14] is restricted to determining the concentration of an element segregated to crystallographically well defined interfaces (e.g. an inversion boundary) and where the solubility of the element in the matrix phase is negligible. In our method there are no such restrictions and furthermore it is possible to extract the change in ELNES (with respect to the matrix phase) of the segregated element.

The aim of this paper is to develop an analytical method that removes the bulk matrix contribution from an EELS measurement acquired from a rough interface using the principles outlined above. The method is applied to the TiN/ poly-Si interface in a HfO_2-based high- *k* dielectric gate stack that has been well characterised using the MLLS technique [6] and is therefore an excellent example to assess the validity of our method. In section 2 of this paper, the background theory to the analytical model is presented, in section 3 the experimental details are given and in section 4 the technique is applied to the Si- $L_{2,3}$, N- K and Ti- $L_{2,3}$ EELS edges at the TiN/ poly-Si interface. Section 5 contains a discussion of the results and identifies some practical limitations as well as potential applications of the technique in other areas of materials characterisation such as core-shell nanoparticles.

2. Background theory to the analytical method

It is easiest to describe the technique by selecting a specific example. Figure 1 is a schematic of the interface between TiN and poly-Si in a HfO_2- based high- *k* dielectric gate stack. The interface is rough and contains an 'interfacial layer' due to (say) the presence of oxygen. Here 'interfacial layer' refers to the region at the interface that has a different ELNES compared to that of the bulk matrix. The origin of the ELNES change can be a chemical reaction, interdiffusion, the change in atomic coordination at the interface or a combination of such effects. Let us assume that it is required to determine the bonding environment of silicon at the TiN/ poly-Si interface using the near edge fine structure of the Si- $L_{2,3}$ EELS edge. For a thin foil, the measured Si- $L_{2,3}$ edge from an analysis volume V_{total} is given by:

$$S(E) = V_i I(E) + V_m M(E) \qquad \dots (1)$$

Here $S(E)$ is the measured Si- $L_{2,3}$ EELS edge from V_{total} expressed as a function of the energy loss E, $I(E)$ and $M(E)$ are the Si- $L_{2,3}$ EELS edge signal *per unit volume* from the interface and poly-Si matrix while V_i, V_m are respectively the interfacial and matrix volumes within V_{total} (figure 1). The TiN will not contribute a Si- $L_{2,3}$ edge signal to $S(E)$. If the TiN volume within V_{total} is denoted by V_{o}, equation (1) can be rewritten as:

$$\begin{aligned} S(E) &= V_i I(E) + (V_{\text{total}} - V_{\text{o}} - V_i) M(E) \\ &= V_i [I(E) - M(E)] + (V_{\text{total}} - V_{\text{o}}) M(E) \end{aligned} \qquad \dots (2)$$

Equation (2) indicates that for a given energy loss E and constant interfacial volume V_i a plot of $S(E)$ vs. $(V_{\text{total}} - V_{\text{o}})$ is a straight line with gradient $M(E)$ and intercept proportional to the interfacial difference spectrum, $[I(E)\text{-}M(E)]$. For rough interfaces, while the shape of $[I(E)\text{-}M(E)]$ is known, it is not possible to determine $I(E)$ without knowing the value of V_i, since it appears in the intercept in equation (2). Furthermore $I(E)$ and $M(E)$ are the interface and matrix EELS spectra per unit volume rather than per ionised atom. Hence [$I(E)$-$M(E)$] will be sensitive to bonding as well as changes to the composition of the element of interest at the interface. However, if there is only a composition change at the interface with no measurable ELNES change then $I(E)$, and hence [$I(E)$-$M(E)$], will simply be proportional to $M(E)$.

There are two main experimental difficulties that need to be overcome before carrying out the above analysis: (i) V_{total} must be varied while keeping V_i constant and (ii) a suitable method for estimating V_{o} must be established. With spectrum imaging [15] in a STEM, the electron probe is rastered over a region of interest and EELS spectra can be collected at each pixel. Data points for the set of $S(E)$ vs. $(V_{\mathrm{total}} - V_{\mathrm{o}})$ graphs, with constant V_i, can then be obtained from suitable sub-regions within the original spectrum image. One graph can be drawn for each energy loss. To illustrate this more clearly, figure 2(a) shows a high angle annular dark field (HAADF) image of a Si/ SiO_x/ HfO_2/ TiN/ poly-Si gate stack. An EELS spectrum image is acquired across the gate stack along the line indicated in the figure. Figure 2(b) is the HAADF intensity profile along the line used for spectrum imaging. The spectrum image sub-regions R_0, R_1, R_2 etc. in figures 2(a)-2(b) contain identical volumes of TiN/ poly-Si interface (i.e. V_i) and TiN (i.e. V_{o}). Note that in order to maintain constant V_i the left hand boundary of R_0, the smallest sub-region, must be within the bulk poly-Si matrix phase and all sub-regions R_0, R_1, R_2 etc. must share a common right hand boundary which is placed within the TiN/ poly-Si interfacial region (see figures 2(a) and 2(b)). The only difference between the sub-regions is in the volume of poly-Si matrix (i.e. V_m). Assuming a constant specimen thickness, V_{total} is proportional to R_i. Hence the integrated signal at a given energy loss, $S(E)$, can be evaluated as a function of R_i and hence V_{total}. Moreover, if V_{o} could be estimated, the integrated signal from the sub-regions from a single spectrum image can be used as data points for a set of $S(E)$ vs. $(V_{\mathrm{total}} - V_{\mathrm{o}})$ graphs.

The spectrum images used in this study are in the form of line profiles across the gate stack as indicated in figure 2(a). In this case V_{total}, V_{o}, V_i and V_m correspond to thin slices through the foil thickness 't' with cross-sectional areas Lt, A_{o}, A_i and A_m, respectively (see figure 1 for a pictorial description of the terms; 'L' is the length of the scanned region). For a line spectrum image equation (2) therefore becomes:

$$S(E) = \lambda A_i[I(E) - M(E)] + \lambda(Lt - A_{\mathrm{o}})M(E) \qquad \ldots (3)$$

Here λ is a parameter that denotes the in-foil dimension of the analysis volume in a direction normal to the line scan direction (figure 1). Equation (3) indicates that a plot of $S(E)$ vs. $(Lt$-$A_{\mathrm{o}})$ for a line spectrum image is also a straight line with gradient proportional to $M(E)$ and intercept proportional to [$I(E)$-$M(E)$]. As indicated previously, sub-regions within the original spectrum image are used as individual data points for the $S(E)$ vs. $(Lt$-$A_{\mathrm{o}})$ plot provided the area A_{o} can be estimated. For thin crystals oriented along non-channeling orientations, the HAADF image intensity varies linearly with specimen thickness and increases monotonically with average atomic number. In figure 3, which plots the HAADF intensity across the gate stack, the bulk TiN layer has a higher HAADF intensity compared to the bulk poly-Si layer due to its larger average atomic number. Furthermore, the intensity across the TiN/ poly-Si interface varies smoothly between these two bulk values as the volume fraction of TiN to poly-Si through the thickness of the foil changes with position. Now consider the infinitesimal column located at the TiN/ poly-Si interfacial region in figure 3. The measured HAADF intensity at this infinitesimal column is I_{col} and the thickness of TiN within the column is t_{o}. The TiN will therefore contribute an intensity $(t_{\mathrm{o}}/t)I_{\mathrm{TiN}}$ to I_{col}, where I_{TiN} is the HAADF intensity of the bulk TiN phase within a similarly sized infinitesimal column ('t' is the foil thickness). This follows from the linear dependence of the HAADF image intensity with respect to specimen thickness for a given atomic number. Neglecting the contribution from the interfacial layer, the HAADF intensity from the poly-Si phase present within the infinitesimal column is $[(t-t_{\mathrm{o}})/t]I_{\mathrm{poly\text{-}Si}}$, where $I_{\mathrm{poly\text{-}Si}}$ is defined in a similar manner to I_{TiN}. Since the interfacial layer thickness is generally much smaller than the combined thickness of the TiN and poly-Si phases we have:

$$I_{\mathrm{col}} = \left(\frac{t_{\mathrm{o}}}{t}\right) I_{\mathrm{TiN}} + \left(\frac{t-t_{\mathrm{o}}}{t}\right) I_{\mathrm{poly\text{-}Si}}$$

$$\text{or} \quad t_{\mathrm{o}} = t\left(\frac{I_{\mathrm{col}} - I_{\mathrm{poly\text{-}Si}}}{I_{\mathrm{TiN}} - I_{\mathrm{poly\text{-}Si}}}\right) \qquad \ldots\ (4)$$

Equation (4) can be used to calculate 't_{o}' for all infinitesimal columns within the interface region and thereby estimate A_{o}, the cross-sectional area of TiN within the analysis region 'Lt'. Spreading of the electron probe within the specimen means that equation (4) gives only an approximate value of t_{o} but, as will be shown below, the effects of beam spreading can largely be neglected since the parameter of interest A_{o} is determined by integrating the calculated value of 't_{o}' over the interfacial region. Furthermore since the equation for t_{o} involves subtracting and dividing HAADF intensities it is not required to correct for the black level and gain of the HAADF photomultiplier tube.

When calculating $S(E)$, individual pixels in a spectrum image sub-region are summed to give the total EELS signal for the analysis region. With a convergent STEM probe however, beam spreading within the specimen results in an EELS measurement that is non-localised. Figure 4 is a schematic of the beam spreading for an electron probe positioned at the top of column B (the columns in the figure represent individual pixels in a spectrum image); the probe is brought to a sharp focus at the specimen entrance surface but diverges subsequently with some of its intensity being transferred to neighbouring columns A and C. The EELS measurement from column B therefore contains information from columns A and C. However, $S(E)$ is the measured EELS signal over a given area and is determined by summing spectra from several columns. Inspection of figure 4 indicates that for a probe positioned on the column C the intensity transferred to B is the same as that transferred to C by the probe initially positioned on column B. Hence, from the simple schematic, the total intensity illuminating a given column should be approximately constant and each column would therefore contribute equally to $S(E)$. Strictly speaking, this argument is only valid for columns in the middle of the analysis region. In reality however, beam spreading is affected not only by the convergence angle of the incident probe but also by the mean atomic number of the specimen and so the situation is more complex for a rough interface. This is especially true if there is a large difference in elastic scattering between the phases either side of the interface, such as for example in the TiN/ HfO_2 interface. However, in practice, the results presented in section 4 indicate that beam broadening does not prohibit obtaining useful information from this analytical technique.

3. Experimental details

Si/ SiO_x (1 nm)/ HfO_2 (4 nm)/ TiN (10 nm)/ poly-Si (100 nm) gate stacks were analysed as part of this study. The layer thicknesses are nominal. The processing conditions can be found in [6] and chemical nanoanalysis is described in [6-7]. Cross-section specimens were prepared by the standard method of grinding, dimpling and ion-beam milling to electron transparency. Data was acquired using the aberration corrected STEM microscope at SuperSTEM, Daresbury operating at 100 kV. Aberrations up to 3rd order are corrected using a Nion Mark II Quadrupole- Octupole corrector [16] which results in a probe size of ~0.1 nm and 24 mrad semi-convergence angle. EELS spectra were acquired in spectrum imaging mode using an UHV ENFINA spectrometer at 0.3 eV/ channel dispersion and 19 mrad collection semi-angle. Spectrum images were in the form of linescans across the gate stack with the step size between pixels being either ~0.2 nm or in a few cases ~0.1 nm. The N- K (401 eV), Ti- $L_{2,3}$ (456 eV) and O- K (532 eV) edges were acquired in a single scan while a separate scan was used to acquire the Si- $L_{2,3}$ (99 eV) edges from roughly the same region of the specimen (the separation between the two spectrum images along the direction parallel to the gate stack layers was ~12 nm). The Si- $L_{2,3}$ and N- K edges for amorphous silicon nitride (SiN_y; figures 8(a) and 9(a)) were acquired using an FEI Tecnai F20 FEG TEM operating at 200 kV (further details can be found in [6]). Power law fitting was used to remove the pre-edge background [17]. Only data where the drift rate was negligible (i.e. $\leq$ 0.1 nm/min) were used for analysis. (The drift rate was estimated by comparing HAADF images before and after EELS spectrum imaging).

A separate spectrum image was used to acquire the low loss spectrum from which the thickness variation across the gate stack could be estimated. Unfortunately the low loss spectrum image does not spatially overlap with any of the core loss spectrum images but nevertheless was measured from a similar region of the specimen (the separation along the direction parallel to the gate stack layers is ~4 nm for the Si- $L_{2,3}$ spectrum image and ~16 nm for the spectrum image mapping N, Ti and O). Figure 5 shows the relative thickness (i.e. ratio of thickness to inelastic mean free path) across the gate stack along with the HAADF intensity profile which has been suitably scaled for display purposes. The relative thickness increased from 0.46 to 0.65 across the poly-Si and TiN regions used for data analysis. The inelastic mean free path was estimated using the Digital Micrograph (DM) freeware script 'Mean Free Path Estimator" [18]. For the experimental conditions used the mean free path is approximately 79 nm for bulk Si and 78 nm for bulk TiN phases. Thus there is an increase in thickness from ~37 nm to ~52 nm over the stack. The effect of such a thickness variation will be discussed in section 5.

A DM script was written to carry out the data analysis described in the previous section. In particular, a straight line was fitted to the $S(E)$ vs. $(Lt\text{-}A_o)$ data points using the method of least squares deviation e.g. [19]. Typically 5 data points were used with the increment in '*L*' between neighbouring data points being ~0.6 nm or 3 spectrum image pixels (see section 4.2 for more details on the accuracy and convergence of the analytical technique). The limiting factor for the maximum number of data points is the finite width of the individual layers. The 'goodness of fit' of a straight line least squares fitted to a series of data points is measured by the correlation coefficient, r^2, which increases monotonically with the quality of the fit and has a value of 1 for a perfect fit [19].

4. Results

4.1 *Distribution of elements across the gate stack*

Figure 6 shows normalised line profiles of the Ti, N and O intensities across the gate stack. The distribution of a given element was determined by integrating its background subtracted, core loss signal over a ~45 eV energy window from the edge onset for each pixel in a line spectrum image (note that there may be some Ti L_1 contribution in the O signal). In figure 6, the maximum number of 'counts' for each element has been normalised but there is no correction for the effects of elastic scattering or thickness variation which are the likely reason for the change of the signal level across the TiN layer. The HAADF signal is also superimposed. The HAADF intensity at the poly-Si region has been arbitrarily set to zero and the intensity of the TiN layer normalised to the Ti and N element distribution profiles.

The Ti and N distributions decay slowly to zero due to the roughness of the interfaces and beam spreading. For example at the TiN/ poly-Si interface the Ti and N distributions decrease from the maximum value to zero over a distance of ~3.5- 4 nm. Furthermore the N profile extends further into the poly-Si than the Ti at the point where the O also peaks, corresponding to the SiO_xN_y interfacial layer seen in earlier work [6]. The separation of the N and Ti profiles, at the point where the normalised number of counts has dropped to half the value for bulk TiN, is 0.4 nm. The source of oxygen at this point in the process has been attributed to a tool change between the TiN and amorphous Si depositions [7]. The oxygen profile in the dielectric shows two distinct heights due to the SiO_x and HfO_2 layers of the gate stack. The intensity of the latter is diminished due to significant elastic scattering by the high atomic number HfO_2 to angles outside the EELS spectrometer collection aperture.

Surprisingly the HAADF signal at the TiN/ poly-Si interface overlaps with the N and O profiles but not the Ti profile. The reason for this is currently being investigated. This will introduce an error in calculating A_o (section 2) but its effect is thought to be relatively minor, since the separation of the HAADF trace and Ti profile (≈0.4 nm) is small compared to the length of the shortest sub-region used in the analytical method (i.e. 1.6 nm).

4.2 *Tests on accuracy and convergence of the analytical technique*

In this section, the accuracy of the analytical technique is examined with respect to experimental parameters such as the magnitude of the area A_o, the pixel size of the spectrum image and the division of the data for the least squares fitting procedure. The Si- $L_{2,3}$ edge at the TiN/ poly-Si interface is used for this purpose. Close to the TiN bulk phase, the higher background and presence of the low energy loss Ti M- edge makes extracting the Si- $L_{2,3}$ signal difficult using a common background subtraction window for the entire spectrum image. In fact the extracted signal becomes negative, rather than zero, close to and at the bulk TiN phase. However, recent experimental results [20] indicate that this problem can be virtually eliminated by Fourier-log deconvolving the core loss spectrum to remove multiple inelastic scattering. Unfortunately the fast beam switch [21-22] required for acquiring the low loss region at each spectrum image pixel was not installed on the instrument used in this study. As a result only those pixels in the spectrum image where the extracted Si- $L_{2,3}$ signal was positive were selected for analysis. Furthermore, although the extracted signal is positive, there could still be residual errors in the background subtraction particularly at energy losses much higher than the edge onset.

Figure 7(a) shows a typical correlation coefficient (r^2) plot for least squares fitting at each energy loss within the range of 95-200 eV. The inset is an expanded view of the energy loss region around the Si- $L_{2,3}$ edge onset at 99 eV. At energy losses below 100 eV the r^2-value is less than its ideal value of unity due to residual noise still remaining after background subtraction. However, for energy losses above 100 eV, where the extracted Si- $L_{2,3}$ signal is statistically significant, the r^2 value is one indicating a good linear fit of the experimental data points. Figure 7(b) is a plot of the gradients of the least squares straight line fits to the experimental data at energy losses within the range of 95-200 eV. From equation (3), the gradient term is proportional to $M(E)$ which in this particular case corresponds to the Si- $L_{2,3}$ edge from the poly-Si matrix phase. The standard error for the gradient term at each energy loss is also shown in figure 7(b) and has been multiplied by a factor of 10 for visual clarity. Above the Si- $L_{2,3}$ edge onset the standard error is less than 2% of the value of the gradient which indicates that the extracted matrix spectrum is statistically significant. To determine whether it agrees with physical reality we have also superimposed the measured Si- $L_{2,3}$ edge from the bulk poly-Si matrix phase in figure 7(b). The integrated area of the measured EELS spectrum was normalised to that of the extracted spectrum for a direct comparison of their near edge fine structure. The extracted and measured EELS spectra are qualitatively similar with the difference between the two spectra being no more than 18% of the measured EELS spectrum value at any given energy loss above the edge onset. The value of 18% is almost an order of magnitude larger than the 2% standard error for calculating the matrix spectrum $M(E)$ and is likely to be caused by errors in background subtraction close to the bulk TiN phase with further contributions possibly arising from beam spreading and thickness variations. However, the error is in the form of a systematically varying scaling factor whereas the positions and amplitudes of the features in the fine structure match very well.

Scientifically the most useful result is the interfacial difference spectrum (i.e. $I(E)$-$M(E)$) which is proportional to the intercept of the least squares straight line fitted to the experimental data (equations (2) and (3)). Figure 7(c) shows the values of the intercepts for Si- $L_{2,3}$ at the TiN/ poly-Si interface at each energy loss within the range of 95-200 eV. Some of the important gross features in the ELNES have been labeled as 'α' (~102 eV), 'β' (~106 eV) and 'γ' (~120 eV) in order to aid the discussion. The interfacial difference spectrum is found to be negative for all energy losses. This is not unreasonable since $I(E)$ and $M(E)$ are the interfacial and matrix EELS spectra per unit volume, rather than per ionised atom, so that ($I(E)$-$M(E)$) will be negative if the number of silicon atoms per unit volume at the interfacial layer is less than the bulk poly-Si matrix. This is expected since the interface layer is silicon oxynitride [6] and there are ~26 atoms/nm^3 in SiO_2 and ~41 in Si_3N_4 while there are ~50 in crystalline Si. Also shown in figure 7(c) is the standard error for the intercept (the negative value of the standard error is plotted for a more direct visual comparison). As a fraction of the mean difference signal it is ~15% whereas the equivalent figure for the fractional error on $M(E)$ is only 2%. The absolute value of the error varies smoothly with energy being largest around 120eV. At this level, the data are more than adequate to allow comparison of the gross features in the ELNES.

Before discussing the shape obtained, the effect of the processing parameters is considered. First the role of the area A_o which in our case is due to the presence of the TiN phase within the analysis volume (figure 1) is considered. From figures 2(a) and 2(b) it can be seen that the magnitude of A_o is increased by moving the right hand side boundary of the sub-regions R_0, R_1, R_2 etc. further towards the TiN phase. A larger value of A_o results in an increased volume fraction of interface to poly-Si matrix which reaches a maximum when the boundary is wholly in the TiN. Thus the measured Si- $L_{2,3}$ edge from the individual sub-regions would show larger ELNES variations between them. The analytical technique could therefore be potentially more accurate for larger A_o values. In figure 7(d) the effect of the A_o area on the extracted TiN/ poly-Si interfacial difference spectrum is examined. Results are shown for A_o values of 17, 30 and 38% and were calculated using data from a single line spectrum image. The maximum value of A_o is limited by the requirement of a positive Si- $L_{2,3}$ signal for those spectrum image pixels at or near the TiN/ poly- Si interface. Recall from equation (3) that the intercept of the least squares fitted straight line, which represents the interfacial difference spectrum, contains the interfacial cross-sectional area A_i as part of the proportionality constant. A_i increases monotonically with A_o and the interfacial difference spectra must therefore be scaled in order to make a direct comparison between them. In figure 7(d) this is done by normalising the intensity valley 'α'. The interfacial difference spectra for the different A_o values are in good agreement up to the intensity valley 'γ' but diverge slightly beyond that. One possible reason for the mismatch at high energy loss could be the presence of residual errors in background subtraction for spectra with high A_o values. The standard error for the interfacial difference spectrum, however, did not vary significantly within the range of A_o values used. The gross features of all spectra in figure 7(d) are nevertheless qualitatively similar.

In the least squares fitting, data points from a given spectrum image can be analysed in several different ways. For example, if there are 20 spectrum image pixels beyond the smallest sub-region R_0 (see figures 2(a), 2(b)), then least squares fitting can be carried out by increasing the length of subsequent sub-regions in steps of 4 spectrum image pixels. This gives a total of 6 data points (including the sub-region R_0) for least squares fitting. We could also increase the length of the sub-regions in steps of 2 spectrum image pixels and use more data points (11 in this case) for least squares fitting. The extracted results are virtually independent of the choice of least squares fitting parameters (results not shown). Another parameter that could affect the analysis is the size of a pixel (i.e. spatial resolution) in the spectrum image. This has been examined by analysing data from line spectrum images with pixels sizes of 0.12 and 0.21 nm respectively. Unfortunately the two data sets are from different regions of the same specimen with the 0.12 and 0.21 nm pixel size spectrum images acquired from 25 and 40 nm thick regions respectively. The geometric probe spreading at the exit surface (= $2\alpha_{\text{probe}}t$) is greater than 1 nm for both cases and spans several spectrum image pixels. Figure 7(e) shows the extracted TiN/ poly-Si interfacial difference spectrum for the two datasets with the intensity valley 'α' normalised for a direct comparison. The two spectra have the same basic shape with the peaks and troughs occurring at similar energies but there are differences in their amplitudes. Perfect agreement between the two curves is not expected given the difference in key parameters and different positions on the specimen. However, it shows that the technique is sufficiently robust to extract meaningful data from spectrum image datasets. In the following sections, the technique is used to analyse the Si- $L_{2,3}$, N- K and Ti- $L_{2,3}$ EELS edges at the TiN/ poly-Si interface. To be consistent, analytical results from the specimen region whose elemental distribution is shown in figure 6 are presented but the reproducibility of these results was confirmed using other data sets as well.

4.3 *Si- $L_{2,3}$ edge at the TiN/ poly-Si interface*

Figure 8(a) shows Si- $L_{2,3}$ reference spectra from elemental Si, amorphous SiN_y and high-*k* gate stack SiO_x. The silicon in each case is tetrahedrally coordinated and the electronegativity increases as Si<N<O. Several features are observed with increasing electronegativity of the nearest neighbour to silicon [23]: (i) the first major peak (i.e. peak A) shifts to higher energies (for Si, SiN_y and SiO_x this peak is at ~102, 106 and 109 eV respectively) and (ii) the relative intensity of the first major peak increases with respect to the broad feature at ~125-130 eV. The SiO_x spectrum was acquired from the high- *k* gate stack SiO_x layer and the Si spectrum was acquired from the neighbouring bulk silicon substrate and hence the local specimen thickness for both measurements was ~50 nm. Furthermore both spectra were extracted from the same number of pixels within a single line spectrum image so that the total acquisition time for each spectrum is constant. Hence each is proportional to the number of Si atoms per unit volume and the constant of proportionality is the same if the effect of elastic scattering is ignored. Thus, if they are subtracted to give the (SiO_x-Si) difference spectrum, it should be directly comparable to the TiN/ poly-Si interfacial difference spectrum extracted using the analytical method. In figure 8(b) the (SiO_x-Si) difference spectrum is superimposed along with the TiN/ poly-Si interfacial difference spectrum (figure 7(c)) and a qualitative comparison shows that the former contains the gross ELNES features 'α', 'β' and 'γ' first introduced in figure 7(c). Subtle differences are also observed such as a change in the relative intensities of the valleys 'α' and 'γ' as well as a more negative peak 'β' for the (SiO_x-Si) difference

spectrum. Peak 'β' has also shifted from ~106 eV in the TiN/ poly-Si interfacial difference spectrum to ~109 eV in the (SiO_x-Si) difference spectrum.

In both the TiN/ poly-Si interfacial difference spectrum (figure 7(c)) and the (SiO_x-Si) difference spectrum (figure 8(b)) the intensity valley 'α' at ~102 eV can largely be assigned to the first major peak A in the EELS spectrum for elemental silicon (figure 8(a)). Si-N and Si-O bonds will not contribute significantly at this energy loss since from figure 8(a) the EELS edge onset for SiO_x and SiN_y are chemically shifted to higher energy losses. This offers the possibility of removing the contribution from elemental Si i.e. $M(E)$ in $(I(E)\text{-}M(E))$ obtained from the extracted intercepts. Figure 8(c) shows $I(E)$ extracted using this 'crystalline- Si' method.

$I(E)$ can also be obtained if A_i in equation (3) can be found. In figure 6, the N- profile extends systematically to the left of the Ti- profile in the same way it did in the earlier work on this material [6]. The displacement needed to overlay them is a direct measure of the interface layer width. With this value, A_i can be evaluated so that the intercept value of $\lambda A_i[I(E)\text{-}M(E)]$ can be converted to $\lambda[I(E)\text{-}M(E)]$ and $\lambda M(E)$ from the slope added to give $\lambda I(E)$. $I(E)$ extracted using this 'displacement' method is also plotted on figure 8(c) and shows all the features present in that from the earlier method. However, it should be noted that the displacement is obtained from the line spectrum image containing the N and Ti edges and this was recorded at a different position on the interface than the line spectrum image containing the Si edge. Nonetheless, the agreement between the two $I(E)$ shapes is quite good in terms of the fine structure if not in terms of the absolute intensities. For comparison, the Si- $L_{2,3}$ edges from SiO_x and SiN_y are also plotted on figure 8(c). The SiO_x edge was obtained from the spectrum image acquired across the high- k gate stack itself while the SiN_y spectrum was acquired from amorphous SiN_y under different experimental conditions (i.e. different operating voltage, collection angle etc.; see section 3). The integrated intensities of all spectra in figure 8(c) have been normalised. Figure 8(d) shows MLLS fits of the SiO_x and SiN_y to the two $I(E)$ shapes. The energy window used for MLLS fitting ranged from 103 to 140 eV. The fits are satisfactory indicating an interfacial silicon oxynitride layer as found in earlier work [6]. The fit coefficients give SiO_x to SiN_y ratios of 1.0 and 1.2 respectively for the first and second methods of obtaining $I(E)$.

As a cross-check, the MLLS fitting method of MacKenzie *et al.* [6] was applied to the Si- $L_{2,3}$ spectrum image using Si- $L_{2,3}$ edges from bulk Si, SiO_x and SiN_y as the reference spectra. The edge for bulk Si was taken from the spectrum image itself while those for SiO_x and SiN_y were those used above. The MLLS fit coefficients for SiO_x and SiN_y showed coincident peaks at the TiN/ poly-Si interface, again consistent with a silicon oxynitride interfacial layer [6]. At the peak position, the SiO_x to SiN_y MLLS fit coefficient ratio was 1.6. This is somewhat larger than the two ratios obtained above and is probably due to systematic errors in deriving $I(E)$, such as a non-uniform specimen thickness (section 5) as well as errors in estimating A_i. The MLLS analysis in [6] showed a ratio close to unity in the region studied. A detailed quantitative study of the homogeneity along the TiN/ poly-Si interface has unfortunately not been carried out and is beyond the scope of this paper.

4.4 *N- K edge at the TiN/ poly-Si interface*

Figure 9(a) shows the N- K EELS edge spectra for the bulk TiN and amorphous SiN_y phases plotted as the intensity per unit volume. The crystallography of the cubic TiN and hexagonal β-Si_3N_4 phases were used to estimate the number of nitrogen atoms per unit volume in each phase. The TiN spectrum was extracted from the spectrum image acquired across the high- *k* gate stack while the SiN_y spectrum was acquired under different experimental conditions (section 3). Peaks in the TiN spectrum are labeled using numerical characters according to the scheme given in [24]. It should be noted that for the TiN spectrum in figure 9(a) the peak doublet 1 and 2 is unresolved and has less intensity than peak 4 although previously published spectra for stoichiometric TiN show the opposite trend [24-25]. This is partly due to multiple inelastic scattering (the specimen thickness was approximately half the inelastic mean free path). The SiN_y spectrum is chemically shifted to higher energy losses and has maximum intensity at ~405 eV (peak A). This is followed by a much broader peak B at ~422 eV. The overall shape of the SiN_y spectrum is similar to that for crystalline Si_3N_4 published in the literature [26-27].

Figure 9(b) shows the TiN/ poly-Si interfacial difference spectrum for the N- K edge extracted using the analytical technique. The calculation method is similar to that described for the Si- $L_{2,3}$ edges at the same interface (section 2) except that the extracted spectrum image sub-regions extend into the TiN matrix phase rather than poly- Si (cf. figures 2(a) and 2(b)). The important gross features of the interfacial difference spectrum are the intensity valley 'α' at ~398 eV and the two peaks 'β' and 'γ' at ~404 and 420 eV respectively. A comparison with the N- K edge for bulk TiN, which is superimposed in figure 9(b), shows that the intensity valley 'α' coincides with the peak doublet 1 and 2 of the TiN spectrum. Similarly the positions of peaks 'β' and 'γ' in the interfacial difference spectrum corresponds to the prominent intensity troughs in the TiN spectrum. The standard error of the interfacial difference spectrum is also shown in figure 9(b). At energy losses greater than the peak 'β' the standard error is no more than 18% of the value of the interfacial difference spectrum; this is a similar error to that for the Si- $L_{2,3}$ edges interfacial difference spectrum (figure 7(c)).

The displacement of the N and Ti profiles in figure 6 can be used to estimate A_i and thereby extract the TiN/ poly-Si interface spectrum, $I(E)$, for the N- K edge (see section 4.3). $I(E)$ extracted using this method is shown in figure 9(c) along with the N- K edge from amorphous SiN_y (figure 9(a)). The maximum intensity has been normalised for a direct comparison of the two spectra. Similar ELNES gross features are observed which further suggests an interfacial silicon oxynitride layer [6]. The peak labeled 'A' in the $I(E)$ spectrum has extra intensity at the edge onset compared to SiN_y which could be due to interfacial states within the band gap [9-10] and/ or due to changes in the bonding environment in silicon oxynitride compared to SiN_y. The relative intensity of the broad feature 'B' with respect to 'A' is also higher for $I(E)$ although this could be due to multiple scattering since the two spectra were acquired under different experimental conditions.

4.5 *Ti- $L_{2,3}$ and O- K edges at the TiN/ poly-Si interface*

Previous MLLS fitting results [6] as well as the analytical method indicate that oxygen at the TiN/ poly-Si interface gives rise to silicon oxynitride type bonding. It is also of interest to try to determine whether any of the oxygen has chemically combined with the titanium. In many of the crystalline titanium oxides (e.g. TiO_2 polymorphs, Ti_2O_3 and perovskites such as $SrTiO_3$) the Ti- L_3 and L_2 white lines are crystal field split by ~2 eV [28-30]. Figure 10(a) shows the measured Ti- $L_{2,3}$ EELS spectrum from the bulk TiN phase as well as the extracted TiN/ poly-Si interfacial difference spectrum for the Ti- $L_{2,3}$ edge along with its standard error (the negative value of the standard error is plotted for a more direct visual comparison). The interfacial difference spectrum was extracted using a method similar to that described for the Si- $L_{2,3}$ edge at the same interface (section 2) except that the spectrum image sub-regions extend into the TiN matrix phase rather than poly-Si (cf. figures 2(a) and 2(b)). Since we are primarily interested in the crystal field splitting the energy loss axis in figure 10(a) has been expanded around the Ti- $L_{2,3}$ white line region. The TiN/ poly-Si interfacial difference spectrum shows two distinct intensity valleys at slightly higher energy loss compared to the Ti- L_3, L_2 white lines for the bulk TiN spectrum; for example the first and second intensity valleys are displaced by ~0.6 eV and ~0.9 eV above the L_3 and L_2 white lines respectively. The standard error at the two intensity valleys is no more than 20% of the local value of the interfacial difference spectrum indicating that these are statistically significant features in the spectrum.

To understand the origin of these features a Gaussian curve was fitted to the L_3 and L_2 white lines separately at each pixel in the spectrum image. No correction was made for the continuum intensity present under each white line in the background subtracted spectrum [17, 31]. Figures 10(b), 10(c) and 10(d) plot the peak height, peak centre and full width at half maximum (FWHM) of the Gaussian curves for the L_3 and L_2 white lines as a function of position along the gate stack, respectively. The peak height in figure 10(b) is at its maximum within the bulk TiN layer but decreases continuously across the TiN/ poly-Si and HfO_2/ TiN interfaces. Figure 10(b) can therefore be used as a guide for following the variation in peak centre and FWHM across the gate stack. Figure 10(c) shows that the peak centre for the L_3 and L_2 white lines shift to lower energy loss at the TiN/ poly-Si interface compared to the TiN matrix. For the former, the maximum shift is ~0.6 eV and for the latter it is ~0.5 eV. These absolute energy shifts are similar in magnitude compared to the equivalent shifts observed in figure 10(a) between a normal and differentiated (i.e. difference) spectrum. Figure 10(d) shows that the FWHM of the white lines increase at the TiN/ poly-Si interface with the largest increase for both white lines being ~0.7 eV. We note that strain at the TiN/ poly-Si interface and disorder can each be a source of broadening of the ELNES features.

It must be noted that since the dispersion used to acquire the experimental EELS spectra was set to ~0.3 eV/ channel the energy shifts observed in figures 10(a) and 10(c) as well as the white line broadening observed in figure 10(d) correspond to only a few CCD channels. In such cases stability of the cold field emitter as well as room environment over the period of acquisition can have an important effect on the measurement (the total acquisition time for this particular spectrum image was around 4 minutes). Although the general trends observed in figures 10(b)-10(d) were reproduced in other spectrum images, including those acquired at a higher dispersion of 0.1 eV/ channel, a more systematic approach, in particular using near- simultaneous acquisition of the low- loss and core-loss regions of the EELS spectrum [21-22], is required to unambiguously confirm if these are due to a real physical phenomenon.

The displacement of the N and Ti profiles in figure 6 can be used to estimate A_i and thereby extract the TiN/ poly-Si interface spectrum, $I(E)$, for the Ti- $L_{2,3}$ edge (see section 4.3). The extracted $I(E)$ spectrum is shown in figure 10(e) along with the experimental spectrum for bulk TiN (figure 10(a)). The maximum intensity has been normalised for a direct comparison. The $I(E)$ spectrum is shifted to lower energy loss compared to the experimental TiN spectrum. The shift in the L_3 and L_2 white lines are ~0.9 and ~0.6 eV respectively. However, the white lines are *narrower* in $I(E)$ compared to bulk TiN, with the decrease in FWHM being ~0.6 and ~1.1 eV for L_3 and L_2 respectively. It is unclear if this is due to the assumptions made in the analytical technique, such as a uniform specimen thickness (section 5), or assumptions made in estimating A_i or both. The $I(E)$ spectrum does not show any evidence for crystal field splitting. However, the lack of crystal field splitting is not a sufficient condition to rule out the presence of Ti-O bonds. For example the Ti-O bonds at the interface must have a suitable geometry (e.g. octahedral, tetrahedral coordination) to give rise to strong overlap between the Ti d-orbitals and O p- orbitals that leads to crystal field splitting. Furthermore in the oxide series TiO_2, Ti_2O_3 and TiO the titanium is octahedrally coordinated with the oxygen anions but the measured crystal field splitting decreases monotonically with Ti valence such that in TiO it is hardly apparent in the experimental Ti- $L_{2,3}$ and O- K edges [28, 30]. In addition, if the oxide is amorphous, the effect of crystal field splitting tends to be obscured by the broadening introduced by the disorder [30].

The fine structure of the O- K edge was also examined at the TiN/ poly-Si interface for crystal field splitting [28, 32]. This approach potentially has a few disadvantages such as the measurement being influenced by any surface oxidation as well as errors in background removal due to the underlying Ti- $L_{2,3}$ metal edge. Figure 11 shows the O- K edges measured from the TiN/ poly-Si interfacial layer and the SiO_x layer in the high- *k* gate stack (the integrated intensity of the two edges have been normalised for a direct comparison). Both spectra were extracted from the same spectrum image dataset with the local thickness for the TiN/ poly-Si interfacial region being ~40 nm and that for the SiO_x layer ~50 nm. The O- K edge for SiO_x has an intense peak (labeled A) at ~532 eV followed by a much broader maximum at ~555 eV (labeled B). At the TiN/ poly-Si interface however, the intensity of peak A is diminished although peak B is unaffected. Recall from sections 4.3-4.4 that evidence was found for a silicon oxynitride layer at the TiN/ poly-Si interface. The ELNES changes at the TiN/ poly-Si interface in figure 11 are consistent with experimental measurements and multiple scattering simulations of the O-K edge from sub-stoichiometric silicon oxides [33]. Replacement of some of the oxygen atoms with nitrogen as well as the possibility of silicon dangling bonds within the silicon oxynitride layer could therefore explain the changes to the O- K edges observed in figure 11. Furthermore the widths of peak A for both spectra are similar indicating a lack of crystal field splitting, consistent with results for the Ti- $L_{2,3}$ edge.

5. Discussion and conclusions

An analytical technique for extracting the interfacial difference spectrum from rough interfaces such as those found in high- *k* gate stacks has been developed. The method is based on analysing a series of EELS spectra, obtained from suitable sub-regions of a given spectrum image, that have a variable interface to matrix volume fraction. A unique advantage of this method over multiple linear least squares fitting is that reference spectra from bulk standards are not required. The analytical method was applied to a TiN/ poly-Si interface containing oxygen in a HfO_2- based high- *k* dielectric gate stack with a TiN metal inserted, poly-Si gate electrode. The robustness of the technique was examined with respect to parameters such as the magnitude of the area A_o, pixel size of the spectrum image as well as the division of the data into points for the least squares fitting procedure and found to yield qualitatively consistent results. In particular analysis of the Si- $L_{2,3}$ and N- K EELS edges indicated the presence of a silicon oxynitride layer at the TiN/ poly-Si interface consistent with previous studies using MLLS fitting [6].

Preliminary analysis of the Ti- $L_{2,3}$ edge at the TiN/ poly-Si interface showed the L_3, L_2 white lines to be broadened and chemical shifted to lower energy loss with respect to bulk TiN. The broadening could be due to a number of effects including strain and disorder and no firm conclusions can be drawn. Changes in composition can result in shifts of the edge threshold. For instance, Craven *et al.* [34] showed that the composition across a TiN/ Ti interface correlated with a shift of the Ti- $L_{2,3}$ edge to lower energy loss with decreasing nitrogen concentration. In this TiN/Ti multilayer, the maximum N to Ti atom ratio was ~0.9 and a shift of 0.5 eV, as seen in Figure 10c, occurred after the N to Ti ratio dropped to ~0.7. The TiN in the gate stack studied here is stoichiometric [7]. It is unclear whether N is lost from the TiN at the interface due to the reaction and, if so, whether it is replaced by O to give a cubic Ti(N,O) structure or an amorphous TiO_z. Thus, like the interpretation of the broadening, the interpretation of the chemical shift is unclear.

It is worth discussing at this stage practical limitations to the analytical method as a characterisation tool. First there is the requirement that a suitable number of sub-regions with varying interface to matrix volume fractions be generated from the matrix phase of interest. This may be an issue in some multilayered structures. For example in the analytical model HfO_2 is the matrix phase for analysing the O- K edge at the TiN/ HfO_2 interface in a high- *k* gate stack. However, figure 2(b) shows that the HAADF intensity line trace for the HfO_2 layer, which has a nominal thickness of only 4 nm, plateaus in only a very narrow region thereby severely restricting the number of sub-regions that can be generated. Another limitation is that since equations (1) and (2) account for contributions from only two 'phases' (i.e. $I(E)$ and $M(E)$), the element of interest should be present on only one side of the interface i.e. one matrix phase. Hence, as an example, the O- K edge at the HfO_2/ SiO_x interface cannot be analysed using this technique.

In this paper, the specimen thickness has been assumed to be constant within the region being analysed. However, in practice, there was significant thickness variation in this region (see figure 5). Despite this, the extracted shapes showed a good degree of consistency with what would be expected. In reality, it is very hard to produce a specimen of constant thickness from a multilayer structure containing layers with a large difference both in hardness and sputtering rate, although significant progress has recently been made using focused ion- beam milling techniques [35]. In this situation, the thickness tends to change most rapidly at the interfaces between dissimilar materials, here Si and TiN. For the best results, the sample must also be as thin as possible without surface effects significantly altering the physical properties of the bulk material. A thin specimen has the advantage of reducing the effects of beam spreading, multiple scattering and diffraction contrast, all of which can perturb the data. However, a thin specimen tends to exacerbate the fractional change in thickness across the interface. Changing thickness causes change in the multiple scattering and hence the edge shapes. Multiple scattering also cause background subtraction problems for the Si- $L_{2,3}$ edge in the presence of TiN as noted above. The change in thickness also results in errors in the values of t_0 predicted by equation (4). In addition, it changes the elastic scattering leading to a corresponding change in the intensity of the spectrum entering the spectrometer.

In principle, all of these effects can be taken into account in the processing provided both the low loss and core loss regions of the spectra along with the HAADF signal are recorded with good spatial registration e.g. by using the dual EELS system [22]. The change of edge shape and the background removal problem caused by multiple scattering can be removed by Fourier logarithmic deconvolution while the effect of elastic scattering can be removed by normalisation by the low loss intensity. A fuller discussion of these processes will be given elsewhere [20].

If the HAADF signals $I_{\text{poly-Si}}$ and I_{TiN} are recorded in the bulk materials in regions of thickness $t_{\text{poly-Si}}$ and t_{TiN} respectively, equation (4) can be re-written in terms of $t(x)$ and $t_o(x)$ at position 'x' giving:

$$t_o(x) = \left(I_{\text{col}} - I_{\text{poly-Si}} \frac{t(x)}{t_{\text{poly-Si}}} \right) \Bigg/ \left(\frac{I_{\text{TiN}}}{t_{\text{TiN}}} - \frac{I_{\text{poly-Si}}}{t_{\text{poly-Si}}} \right) \quad \ldots (5)$$

This is no longer simply a ratio of differences in intensity and so the individual intensities need to be corrected for any DC offset i.e. by subtracting the signal recorded through a hole in the specimen under identical conditions. The low loss part of the spectrum gives $t(x)/\lambda(x)$ and $\lambda(x)$ can be obtained from the local composition using the Kramers-Kronig parameterisation method of Malis *et al.* [36]. $t(x)$ and $t_o(x)$ along with the corrected edge shapes can now be used in equation (3) to extract $M(E)$ and $I(E)$.

Even without correction of these effects this analytical method does offer an alternative characterisation tool that complements other established techniques such as MLLS fitting, provided the system meets the criteria noted above. This has been demonstrated for the case of a TiN/ poly-Si interface in a high- k gate stack. Furthermore the general principle can be extended from rough interfaces to characterisation of (say) core-shell nanoparticles. Here an EELS spectrum close to the centre of the nanoparticle will be largely dominated by the core region while the shell has a greater effect as the electron probe is moved further away from the centre. By analysing the changes in the measured EELS spectrum from sub-regions of different radii it is therefore possible to extract the EELS edges from the core and shell regions. This will be the subject of a separate paper.

6. Acknowledgements

The authors would like to thank IMEC for depositing the high- *k* gate stack and Mr. Brian Miller (University of Glasgow) for preparing specimens suitable for electron microscopy. Financial support from EPSRC for the high- *k* project (GR/S44280/01) and SuperSTEM facility (EP/D040205/1) is also greatly appreciated.

7. References

[1] P. S. Lysaght, J. F. Peterson, B. Foran, C. D. Young, G. Bersuker, H. R. Huff, *Materials Science in Semiconductor Processing*, **7** (2004) 259.
[2] A. J. Craven, M. MacKenzie, D. W. McComb, F. T. Docherty, *Microelectronic Engineering*, **80** (2005) 90.
[3] B. Foran, J. Barnett, P. S. Lysaght, M. P. Agustin, S. Stemmer, *J. Electron Spetroscopy and Related Phenomena*, **143** (2005) 149.
[4] M. P. Agustin, L. R. C. Fonseca, J. C. Hooker, S. Stemmer, *Appl. Phys. Lett.*, **87** (2005) 121909.
[5] M. MacKenzie, A. J. Craven, D. A. Hamilton, D. W. McComb, *Appl. Phys. Lett.*, **88** (2006) 022108.
[6] M. MacKenzie, A. J. Craven, D. W. McComb, S. De Gendt, *Appl. Phys. Lett.*, **88** (2006) 192112.
[7] F. T. Docherty, M. MacKenzie, A. J. Craven, D. W. McComb, S. De Gendt, S. McFadzean, C. M. McGilvery, *Microelectronic Engineering*, **85** (2008) 61.
[8] A. J. Craven, M. MacKenzie, D. W. McComb, *Nanoanalysis of high- k dielectrics on semiconductors*, 978-1-4244-2040-7/08, *IEEE* proceedings of 15th IPFA, 2008, Singapore.
[9] D. A. Muller, T. Sorsch, S. Moccio, F. H. Baumann, K. Evans-Lutterodt, G. Timp, *Nature*, **399** (1999) 758.
[10] P. E. Batson, *Nature*, **366** (1993) 727.
[11] N. Daneu, T. Walther, A. Rečnik, *Proceeding of the 15th International Congress on Electron Microscopy vol. 3*, J. Engelbrecht, T. Sewell, M. Witcomb, R. Cross, P. Richards eds., (2002) 63.
[12] T. Walther, N. Daneu, A. Rečnik, *Interface Science*, **12** (2004) 267.
[13] T. Walther, *J. Microsc.* **215** (2004) 191.
[14] T. Walther, *J. Microsc.* **223** (2006) 165.
[15] C. Jeanguillame, C. Colliex, *Ultramicroscopy* **28** (1989) 252.
[16] O. L. Krivanek, N. Dellby, A. R. Lupini, *Ultramicroscopy* **78** (1999) 1.
[17] R. F. Egerton, *Electron Energy-Loss Spectroscopy in the Electron Microscope*, 2nd edition, Plenum Press, New York, 1996.
[18] http://www.felmi-zfe.tugraz.at/dm_scripts/
[19] G. L. Squires, *Practical Physics*, McGraw-Hill, London, 1968.

[20] M. MacKenzie, A. J. Craven, unpublished results.
[21] A. J. Craven, J. A. Wilson, W. A. P. Nicholson, *Ultramicroscopy* **92** (2002) 165.
[22] J. Scott, P. J. Thomas, M. MacKenzie, S. McFadzean, J. Wilbrink, A. J. Craven, W. A. P. Nicholson, *Ultramicroscopy* **108** (2008) 1586.
[23] W. M. Skiff, R. W. Carpenter, S. H. Lin, *J. Appl. Phys.* **58** (1985) 3463.
[24] A. J. Craven, *J. Microsc.* **180** (1995) 250.
[25] A. T. Paxton, M. van Schilfgaarde, M. MacKenzie, A. J. Craven, *J. Phys.: Condens. Matter* **12** (2000) 729.
[26] H. Gu, M. Ceh, S. Stemmer, H. Müllejans, M. Rühle, *Ultramicroscopy* **59** (1995) 215.
[27] H. K. Schmid, *J. Am. Ceram. Soc.* **88** (2005) 404.
[28] E. Stoyanov, F. Langenhorst, G. Steinle-Neumann, *Am. Mineralogist* **92** (2007) 577.
[29] R. Brydson, H. Sauer, W. Engel, J. M. Thomas, E. Zeitler, N. Kosugi, H. Kuroda, *J. Phys.: Condens. Matter* **1** (1989) 797.
[30] T. Manoubi, PhD thesis, Universite de Paris-sud, 1989.
[31] D. H. Pearson, C. C. Ahn, B. Fulz, *Phys. Rev. B* **47** (1993) 8471.
[32] R. Brydson, H. Sauer, W. Engel, F. Hofer, *J. Phys. : Condens. Matter* **4** (1992) 3429.
[33] D. J. Wallis, P. H. Gaskell, R. Brydson, *J. Microsc.* **180** (1995) 307.
[34] A. J. Craven, C. P. Scott, M. MacKenzie, P. Hatto, C. Davies, *Surf. Coat. Tech.* **108-109** (1998) 217.
[35] J. M. Cairney, P. R. Munroe and M. Hoffman, *Surf. Coat. Tech.* **198** (2005) 165.
[36] T. Malis, S.C. Cheng and R.F. Egerton, *J. Elctron. Microsc. Tech.* **8** (1988) 193

Figure Captions

Figure 1: Schematic diagram of a rough TiN/ poly-Si interface containing an interfacial layer. Physical parameters used in the analytical method are as indicated (see text for further details). For analysing the Si- $L_{2,3}$ edge sub-regions of length '*L*' are constructed such that the left hand boundary is within the bulk poly-Si phase and the right hand boundary stays fixed within the TiN/ poly-Si interfacial region. The directions of the specimen thickness '*t*' and the in-foil dimension of the analysis volume 'λ' are also indicated in the figure.

Figure 2: (a) STEM HAADF image of a Si/ SiO_x/ HfO_2/ TiN/ poly-Si gate stack. A spectrum image is acquired across the gate stack along the line indicated in the figure. R_o, R_1, R_2 etc. represent individual sub-regions of the spectrum image used in the analytical method. Figure 2(b) is the HAADF intensity line trace along the spectrum image region shown in figure 2(a). The individual gate stack layers as well as the sub-regions R_o, R_1, R_2 are indicated.

Figure 3: Schematic showing the relationship between the rough interface geometry and measured HAADF intensity. The HAADF intensity increases smoothly from its bulk poly-Si value to the bulk TiN value across the interface due to a gradual increase in the TiN to poly-Si volume fraction. This dependence can be used to determine the volume of TiN and poly-Si within a given analysis region (see text for further details).

Figure 4: Schematic showing the effect of probe spreading through the foil thickness and its effect on the analytical technique. The columns A, B, C etc. represent individual pixels in a spectrum image. The probe centred on column B is shaded grey while the probe centred on column C is represented by the dashed lines. For the former probe more intense shading is used to represent regions with a higher electron current density. See text for further details.

Figure 5: Relative thickness (i.e. ratio of thickness to inelastic mean free path) as a function of position across the gate stack extracted from a low loss spectrum image. Also shown is a suitably scaled HAADF intensity plot for the spectrum image region.

Figure 6: Distribution of the elements titanium, nitrogen and oxygen across the gate stack determined from a single line spectrum image similar to that shown in figure 2(a). The silicon substrate is on the right and the poly-Si layer is to the left of the diagram. The number of counts for each element was determined by integrating the relevant background subtracted EELS signal. The maximum number of counts for each element has been normalised. Oxygen is detected at the TiN/ poly-Si interface. Also shown is the HAADF intensity along the line spectrum image. The HAADF intensity of bulk poly-Si has been arbitrarily set to zero and the intensity of bulk TiN normalised to the N and Ti distribution profiles.

Figure 7: (a) Plot of correlation coefficient as a function of energy loss for the least squares fitting of a straight line during analysis of the Si- $L_{2,3}$ edge at the TiN/ poly-Si interface. The inset shows the graph in more detail for the energy loss range of 95-105 eV. Figure 7(b) shows the extracted and measured Si- $L_{2,3}$ edges for the poly- Si matrix phase. The former was determined by the analytical method using data from the TiN/ poly-Si interface region. The integrated area of the measured spectrum was normalised to that of the extracted spectrum. Also shown is the standard error for the extracted Si- $L_{2,3}$ spectrum multiplied by a factor of x10 for visual clarity. In figure 7(c) the extracted TiN/ poly-Si interfacial difference spectrum for the Si- $L_{2,3}$ edge is shown along with its standard error. The negative of the standard error is plotted for a more direct visual comparison. Important gross features in the interfacial difference spectrum have been labeled as ‘α’, ‘β’ and ‘γ’. Figures 7(d) and 7(e) show the effect of TiN cross-sectional area A_o within the analysis region and spectrum image pixel size on the extracted TiN/ poly-Si interfacial difference spectrum for the Si- $L_{2,3}$ edge. The spectra have been normalised to the intensity valley labeled ‘α’ at ~102 eV.

Figure 8: (a) Si- $L_{2,3}$ edge shapes for elemental Si, amorphous SiN_y and gate stack SiO_x phases. Figure 8(b) shows the experimental (SiO_x-Si) difference spectrum for the Si- $L_{2,3}$ edge plotted as the intensity per unit volume. The TiN/ poly-Si interfacial difference spectrum (figure 7(c)) is also superimposed. Figure 8(c) shows the TiN/ poly-Si interfacial spectrum, $I(E)$, extracted using the ‘crystalline- Si’ and ‘displacement’ methods (see text for further details). Si- $L_{2,3}$ spectra from bulk SiN_y and SiO_x phases are also shown in the figure. The integrated intensities of all spectra in figure 8(c) have been normalised. Figure 8(d) shows the two $I(E)$ spectra along with the best MLLS fit using the SiO_x and SiN_y edges as reference spectra.

Figure 9: (a) Experimental N- K edge shapes for TiN and amorphous SiN_y phases plotted as the intensity per unit volume. Peaks in the TiN spectrum are labeled using numeric characters while Latin letters are used for the SiN_y spectrum. Figure 9(b) shows the TiN/ poly-Si interfacial difference spectrum for the N- K edge extracted using the analytical method along with its standard error. Important gross features are labeled as ‘α’, ‘β’ and ‘γ’. The N- K edge for bulk TiN is also superimposed in figure 9(b). Figure 9(c) shows the TiN/ poly-Si interface spectrum, $I(E)$, for the N- K edge extracted using the ‘displacement’ method along with the amorphous SiN_y spectrum from figure 9(a). The maximum intensity has been normalised.

Figure 10: (a) Ti- $L_{2,3}$ edge measured from bulk TiN and TiN/ poly-Si interfacial difference spectrum for the Ti- $L_{2,3}$ edge extracted using the analytical technique. The standard error for the latter is also shown; the negative of the standard error is plotted for a more direct visual comparison. Figures 10(b), 10(c) and 10(d) plot the peak height, peak centre and peak full width at half maximum (FWHM) of the ‘best-fit’ Gaussian curve used to model the Ti- L_3 and L_2 white lines as a function of position across the gate stack. The approximate positions of the bulk TiN phase as well as HfO_2/ TiN and TiN/ poly-Si interface regions are indicated in each figure. Figure 10(e) shows the TiN/ poly-Si interface spectrum, $I(E)$, for the Ti- $L_{2,3}$ edge extracted using the ‘displacement’ method. The Ti- $L_{2,3}$ edge for bulk TiN is also superimposed and the maximum intensity has been normalised.

Figure 11: Experimental O- K edges from the gate stack SiO_x layer and at the TiN/ poly-Si interface. The integrated intensity has been normalised for the two spectra. Important gross features are labeled as ‘A’ and ‘B’.

Figure

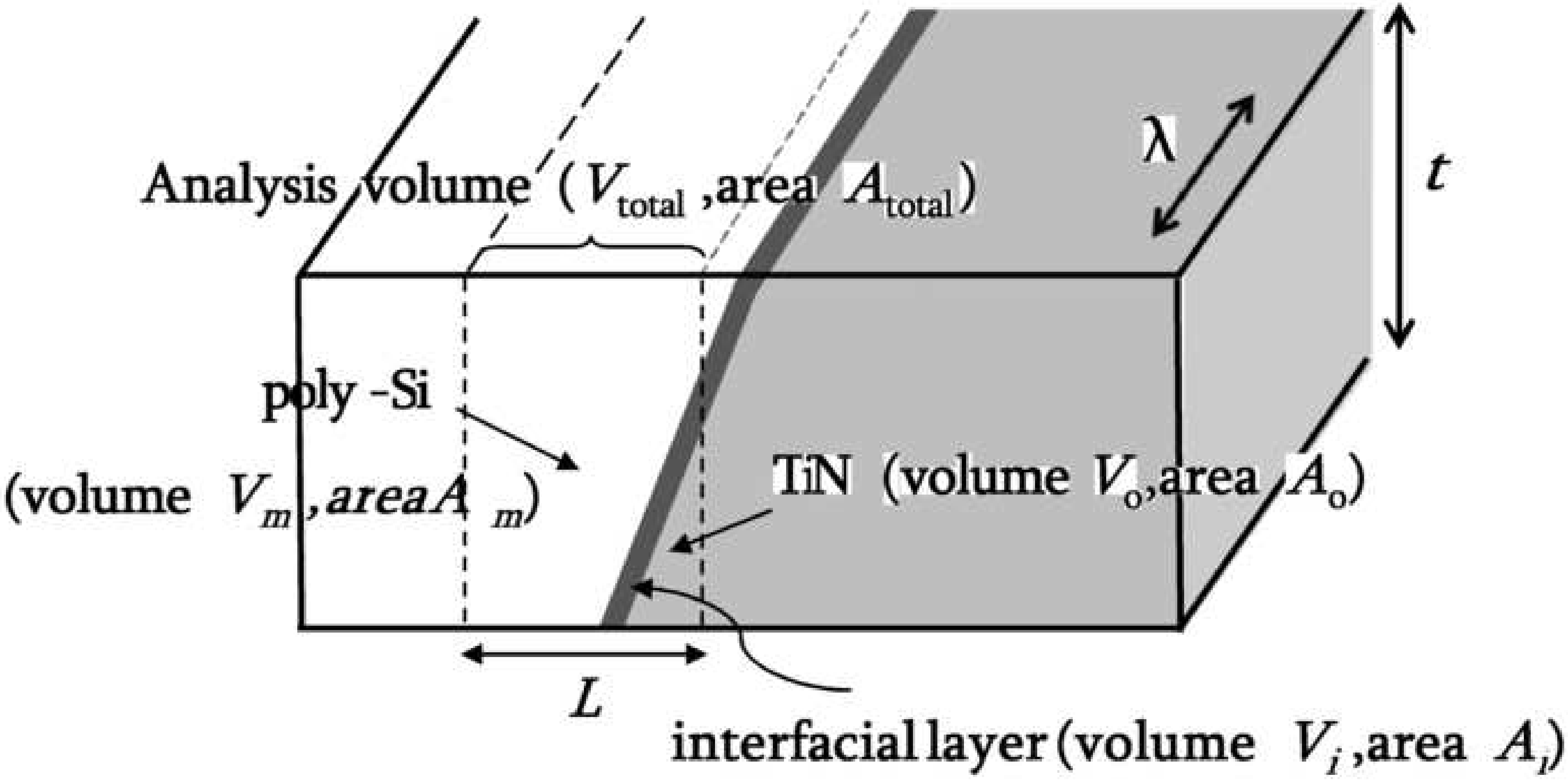
Analysis volume (V_{total} ,area A_{total})
λ
t
poly -Si
(volume V_m ,area A_m)
TiN (volume V_o,area A_o)
L
interfacial layer (volume V_i ,area A_i)

Figure

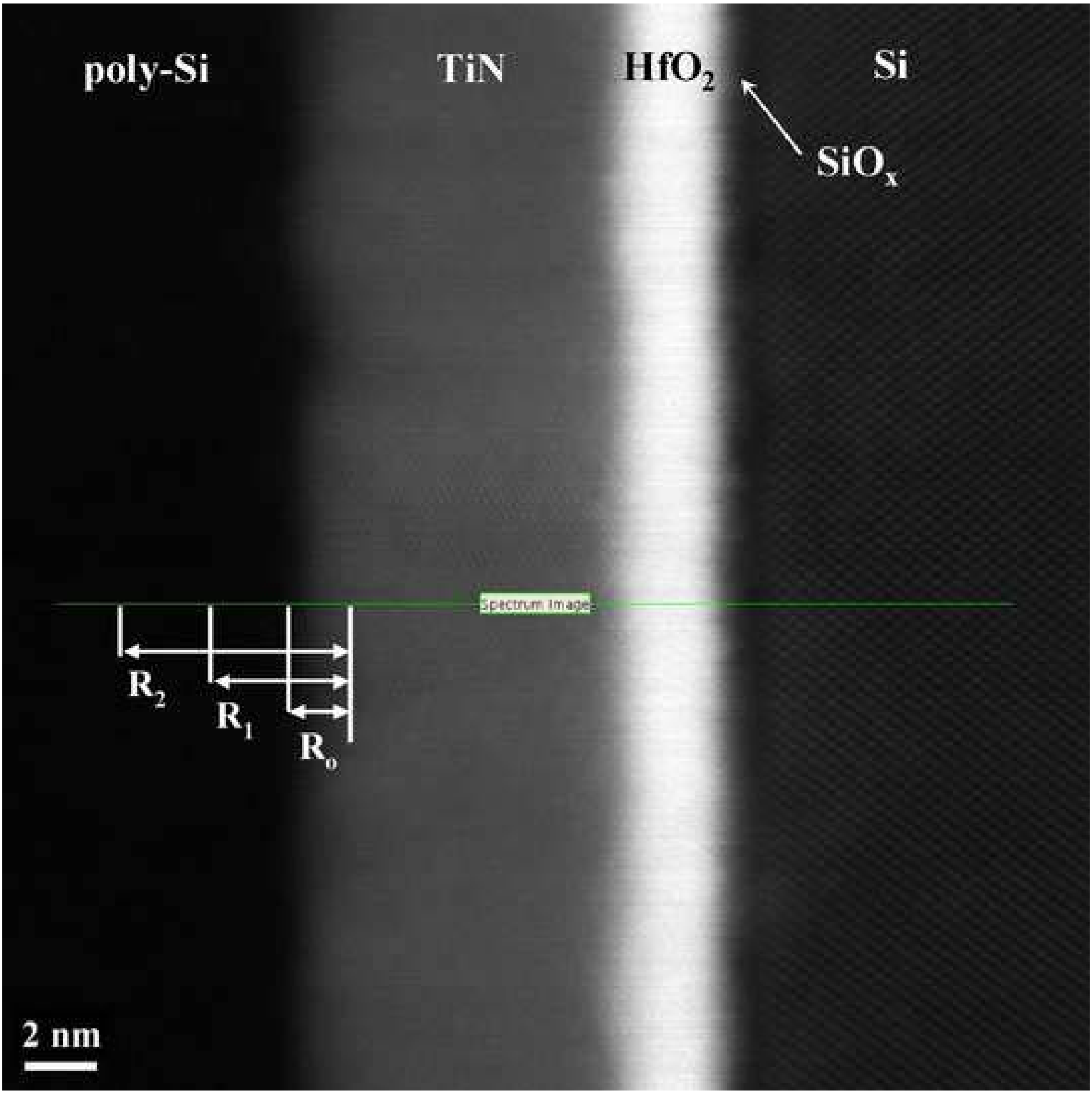
poly-Si
TiN
HfO_2
Si
SiO_x
Spectrum Image
R_2
R_1
R_0
2 nm

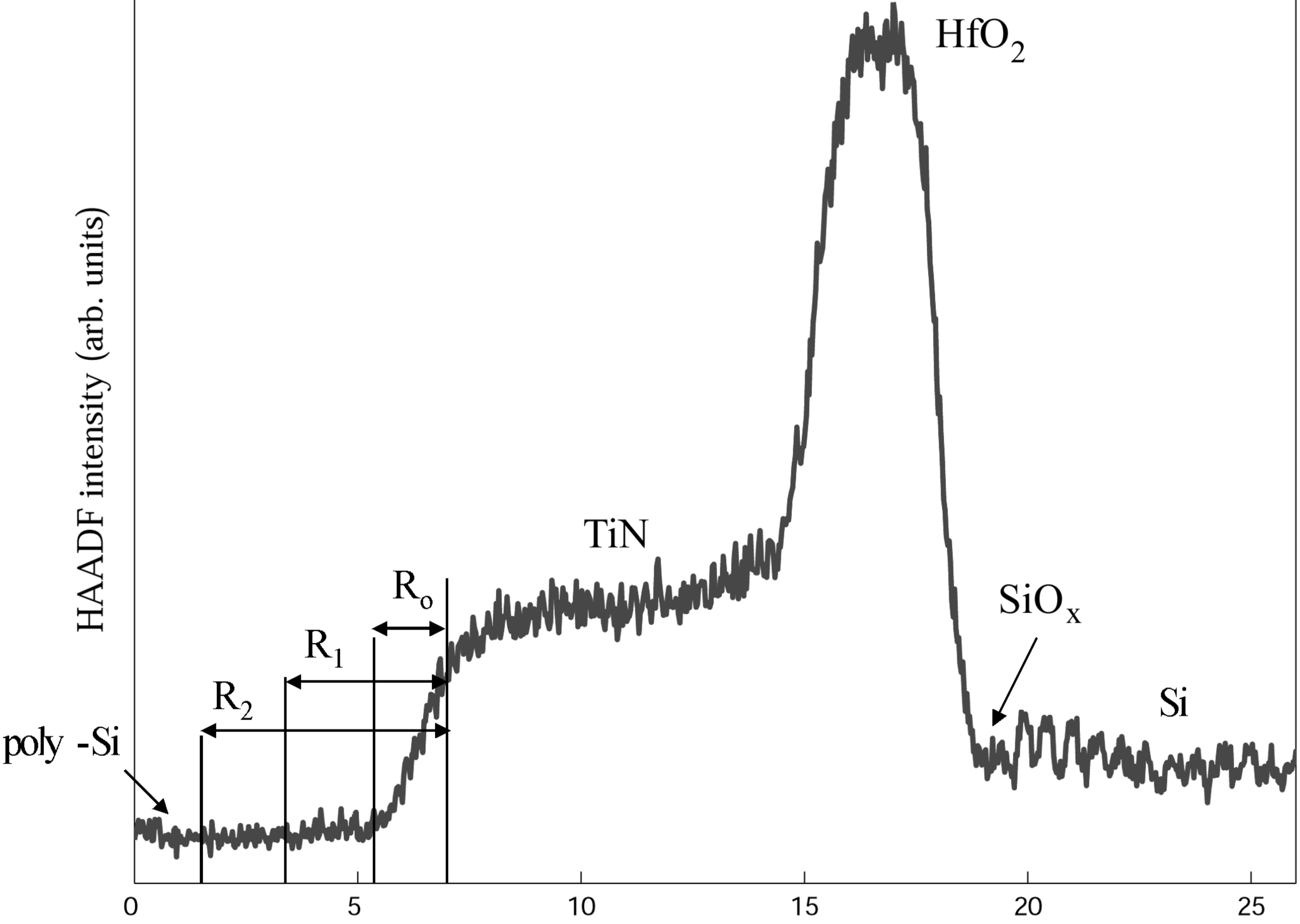
HfO$_2$
HAADF intensity (arb. units)
TiN
R$_o$
R$_1$
R$_2$
SiO$_x$
Si
poly -Si
0
5
10
15
20
25

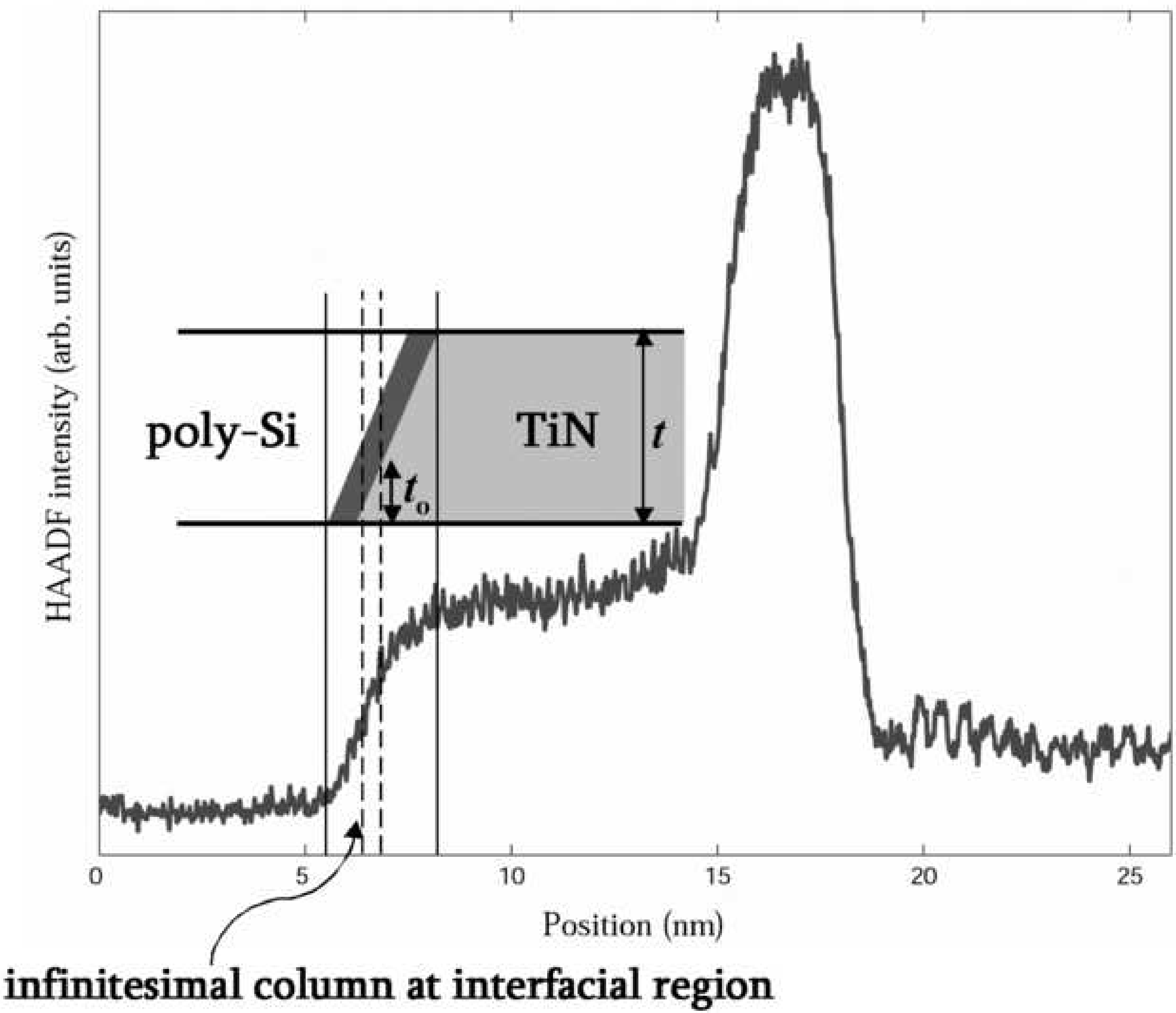
HAADF intensity (arb. units)
Position (nm)
0
5
10
15
20
25
poly-Si
TiN
t
t_o
infinitesimal column at interfacial region

Figure

Click here to download high resolution image

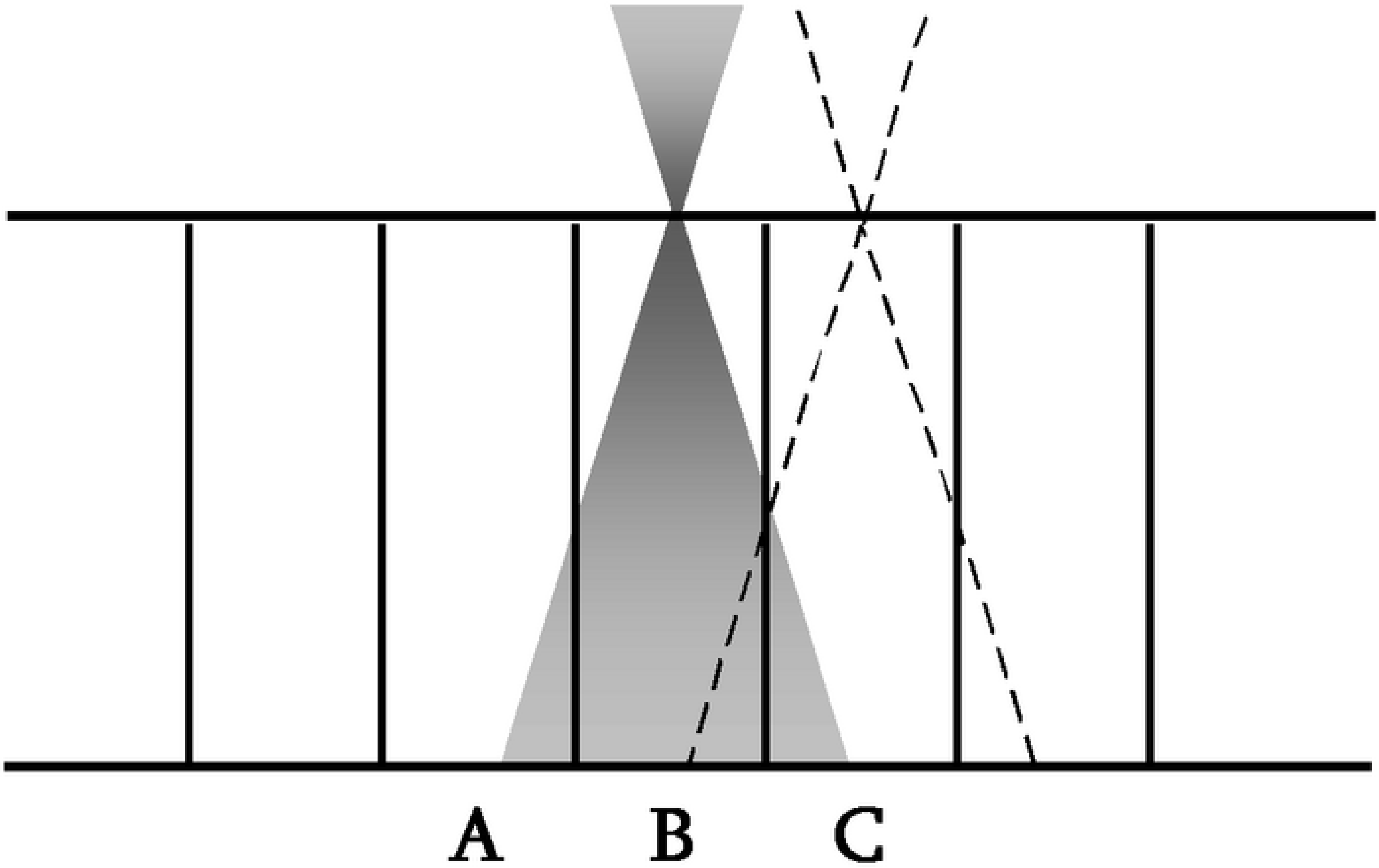

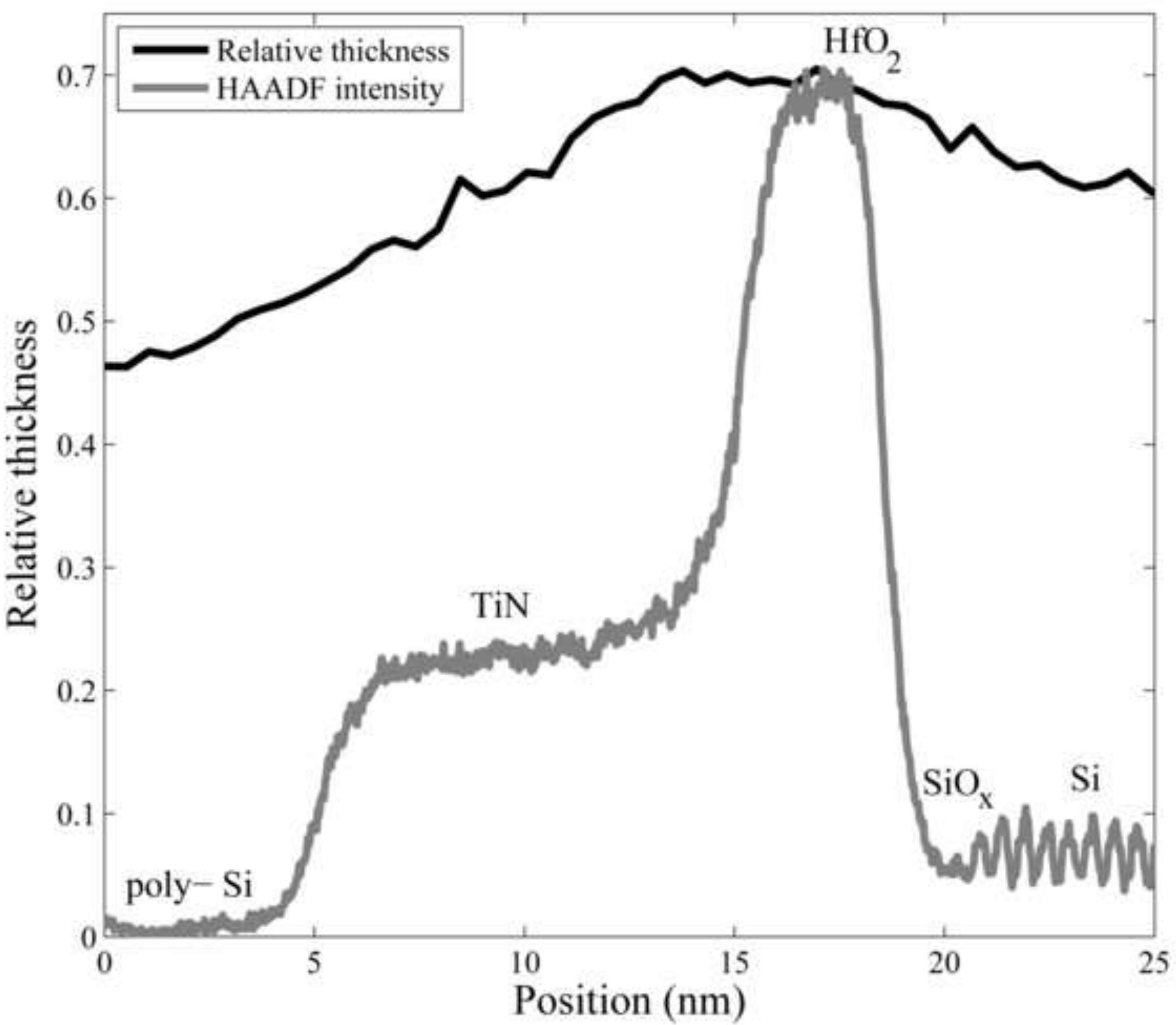
Relative thickness
HAADF intensity
HfO$_2$
TiN
poly− Si
SiO$_x$
Si
Relative thickness
0
0.1
0.2
0.3
0.4
0.5
0.6
0.7
0
5
10
15
20
25
Position (nm)

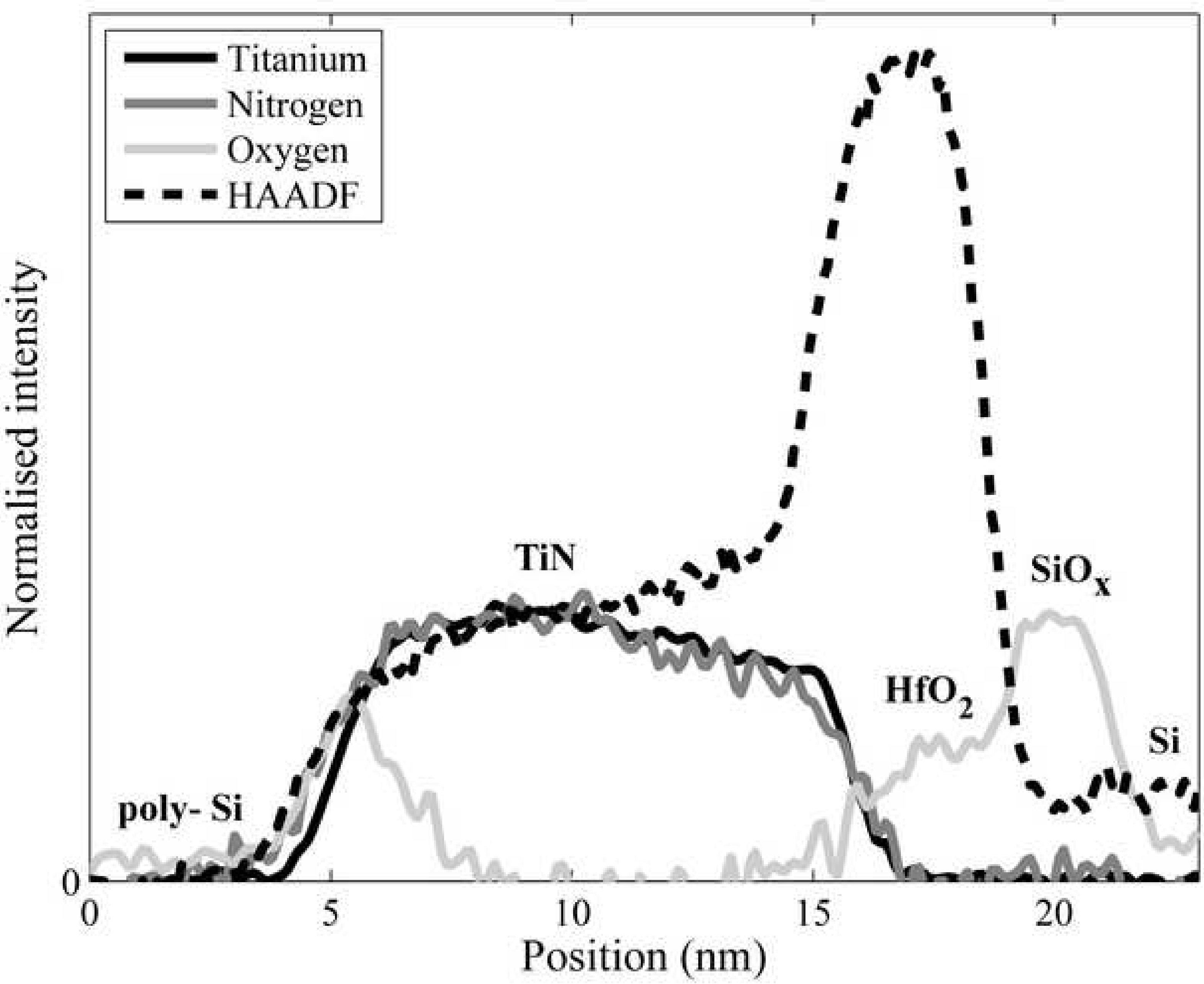
Titanium
Nitrogen
Oxygen
HAADF
Normalised intensity
Position (nm)
0
0
5
10
15
20
poly- Si
TiN
HfO_2
SiO_x
Si

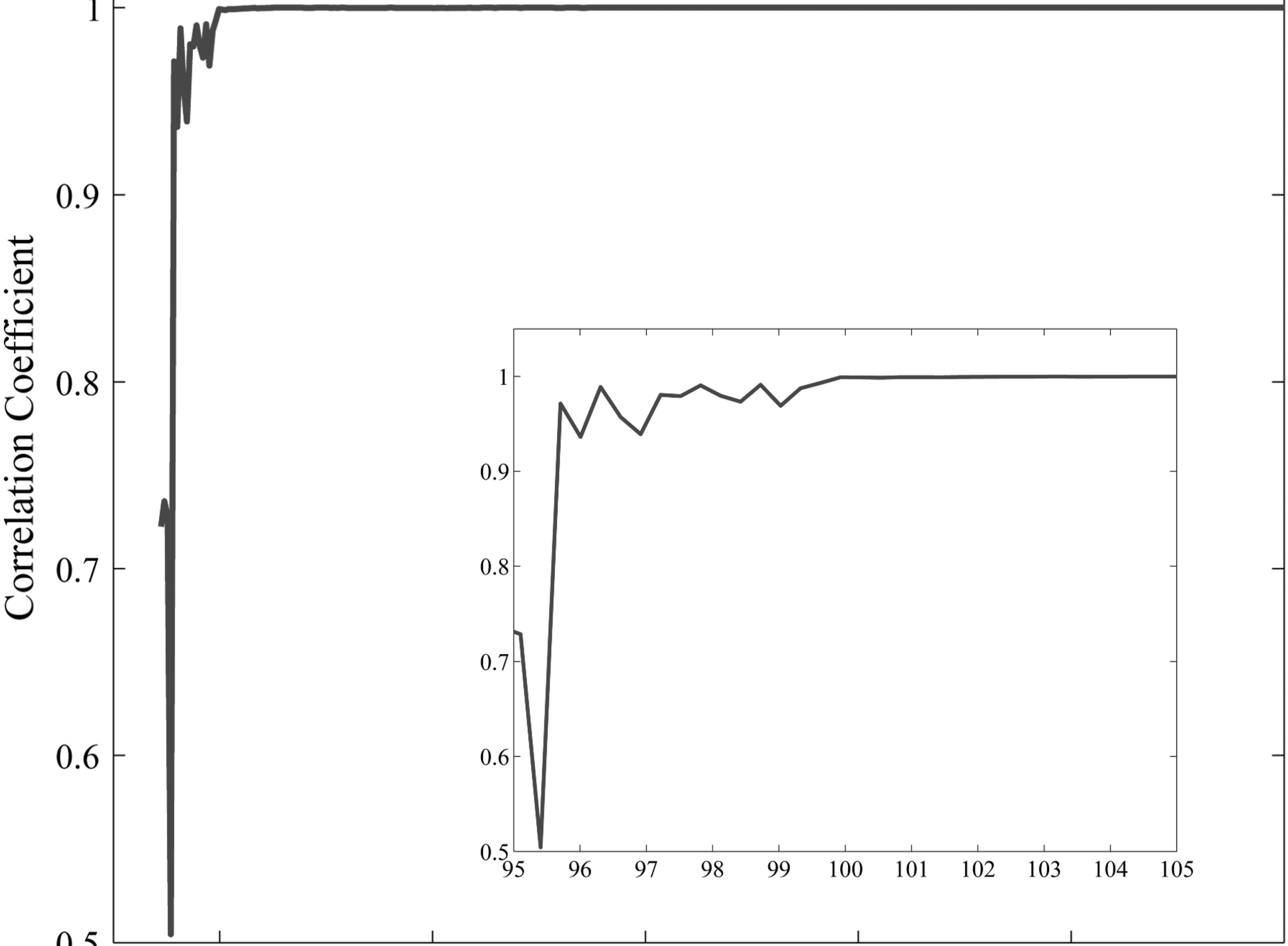
Correlation Coefficient
1
0.9
0.8
0.7
0.6
0.5
1
0.9
0.8
0.7
0.6
0.5
95
96
97
98
99
100
101
102
103
104
105

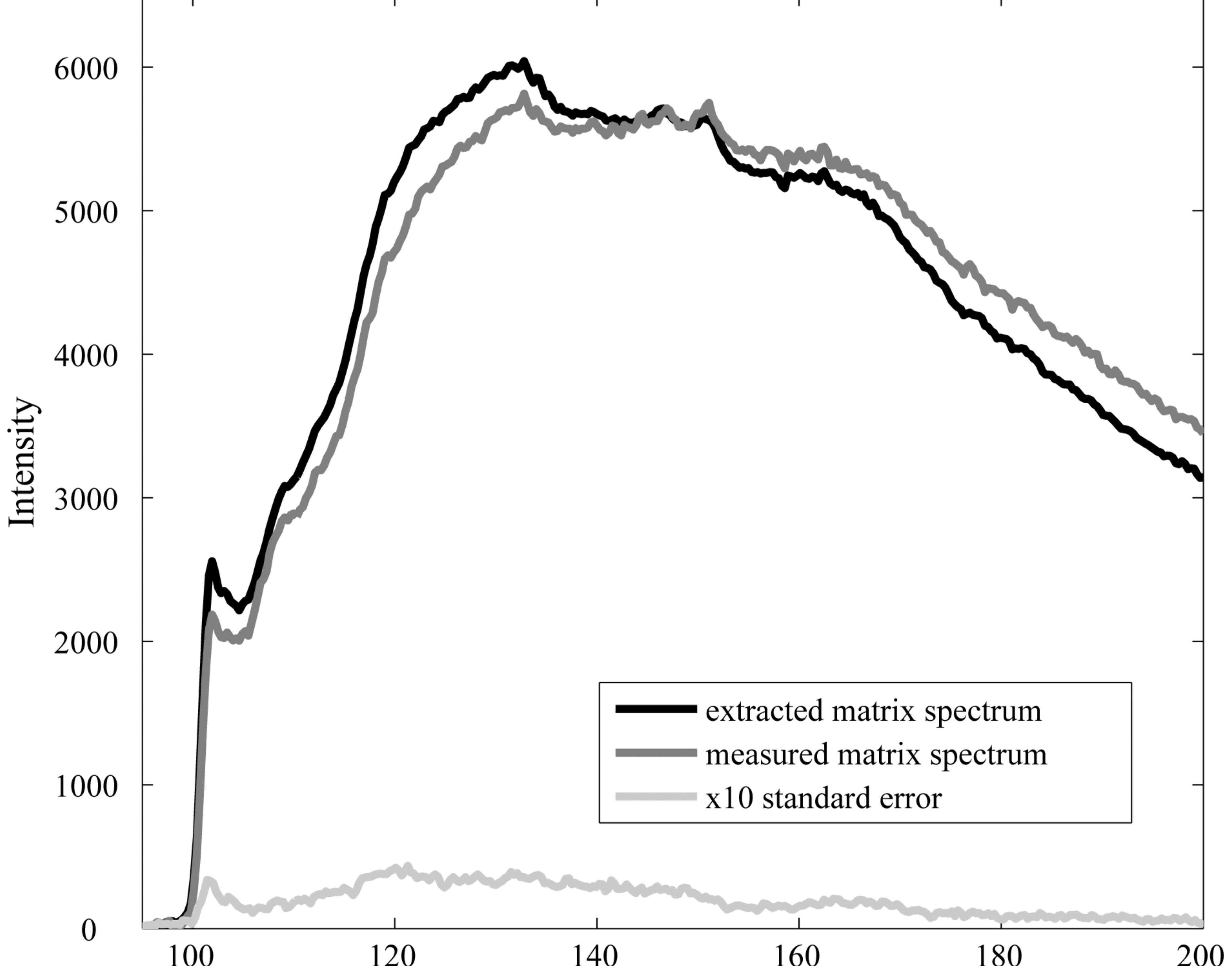
Intensity
6000
5000
4000
3000
2000
1000
0
100
120
140
160
180
200
extracted matrix spectrum
measured matrix spectrum
x10 standard error

Figure

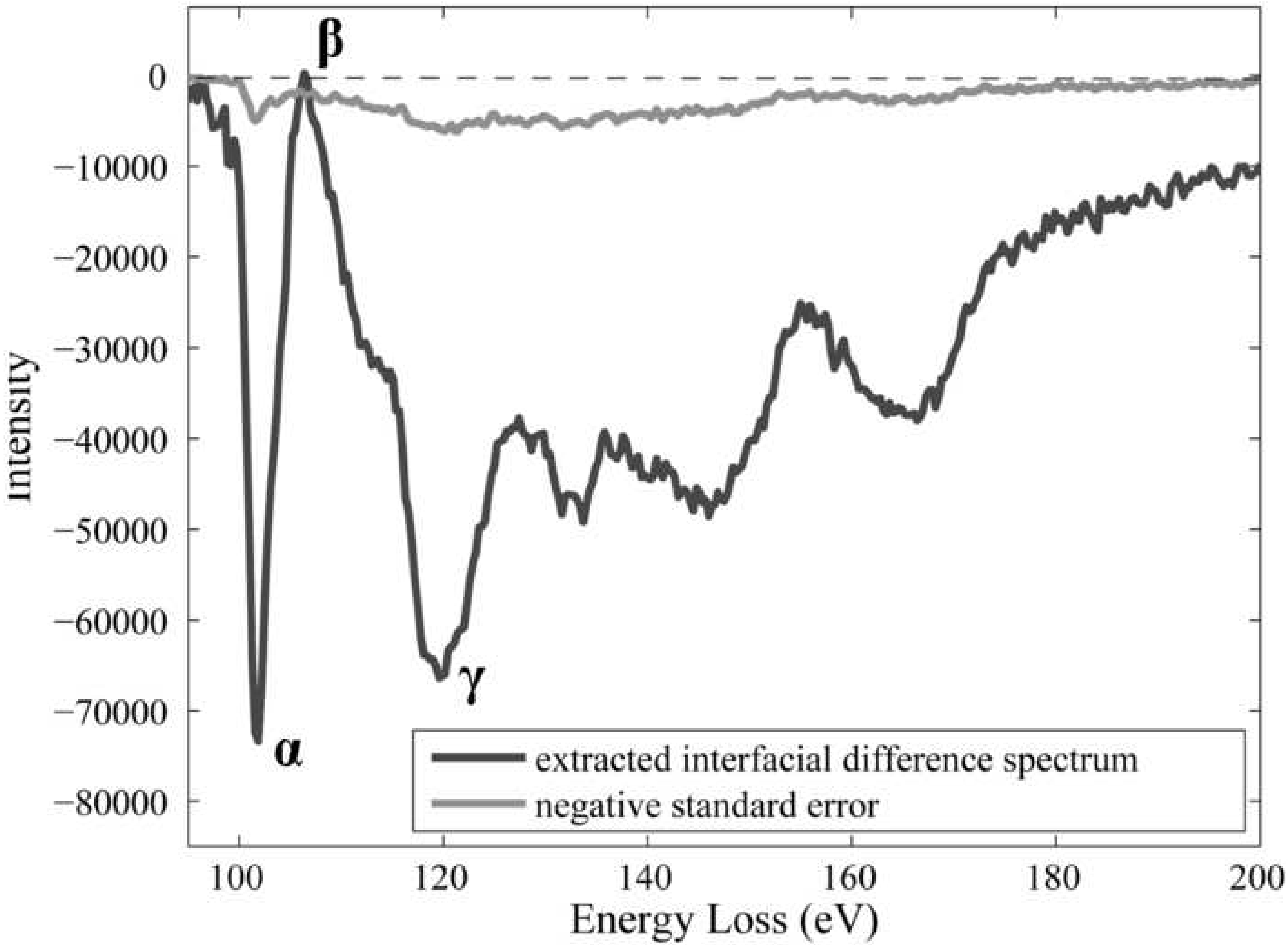
β
0
−10000
−20000
−30000
−40000
−50000
−60000
−70000
−80000
Intensity
γ
α
extracted interfacial difference spectrum
negative standard error
100
120
140
160
180
200
Energy Loss (eV)

Figure
Click here to download high resolution image

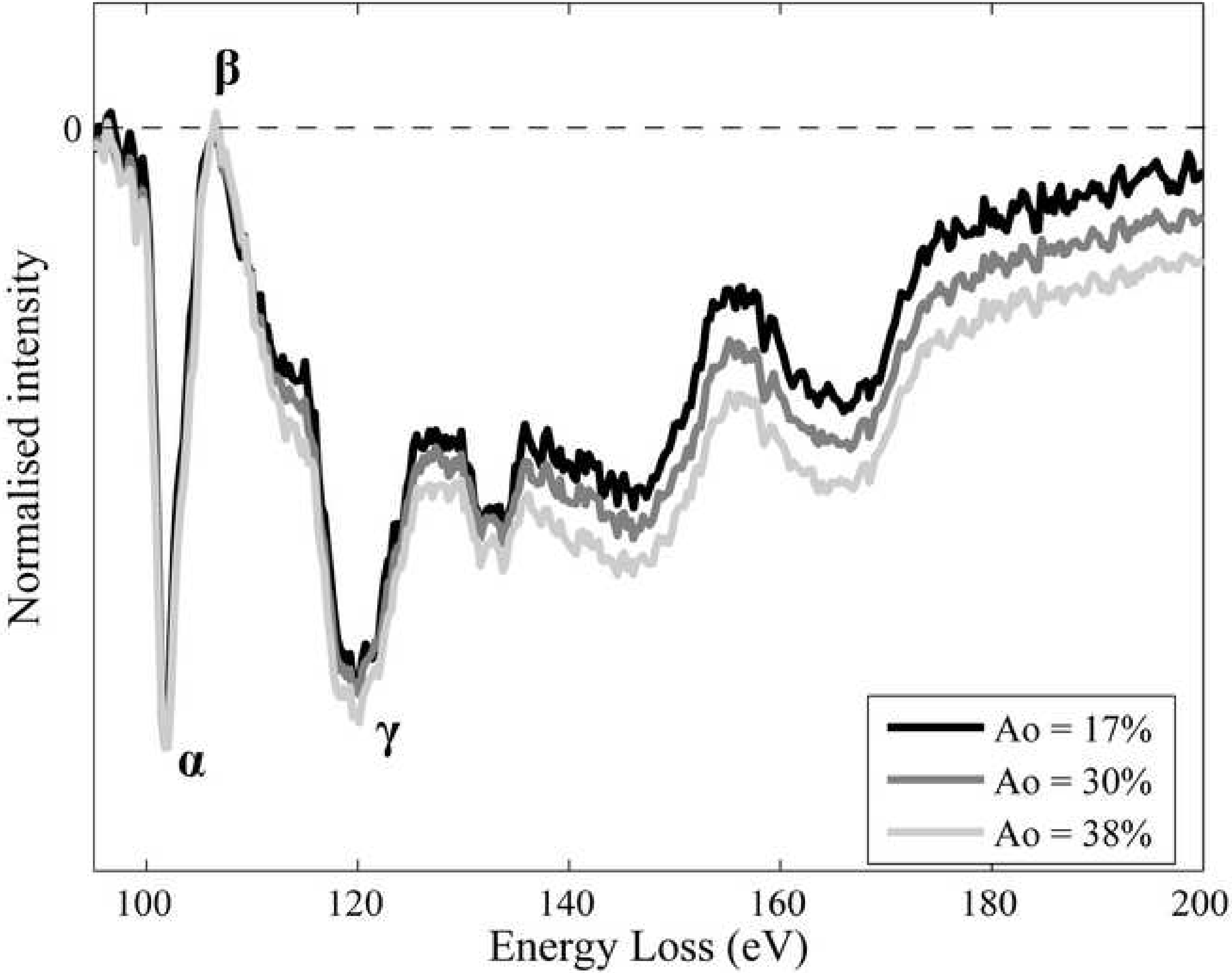

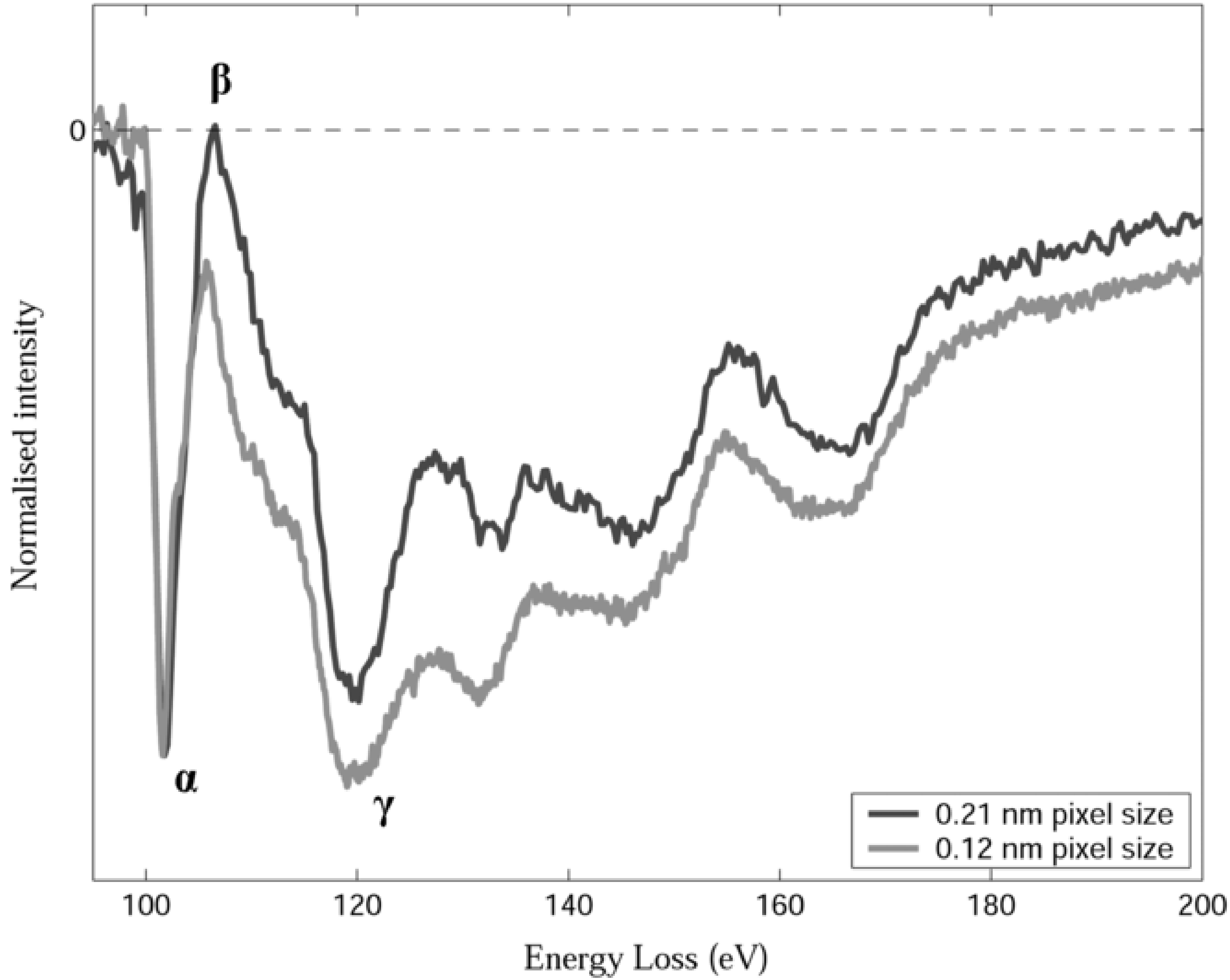
β
0
α
γ
Normalised intensity
100
120
140
160
180
200
Energy Loss (eV)
0.21 nm pixel size
0.12 nm pixel size

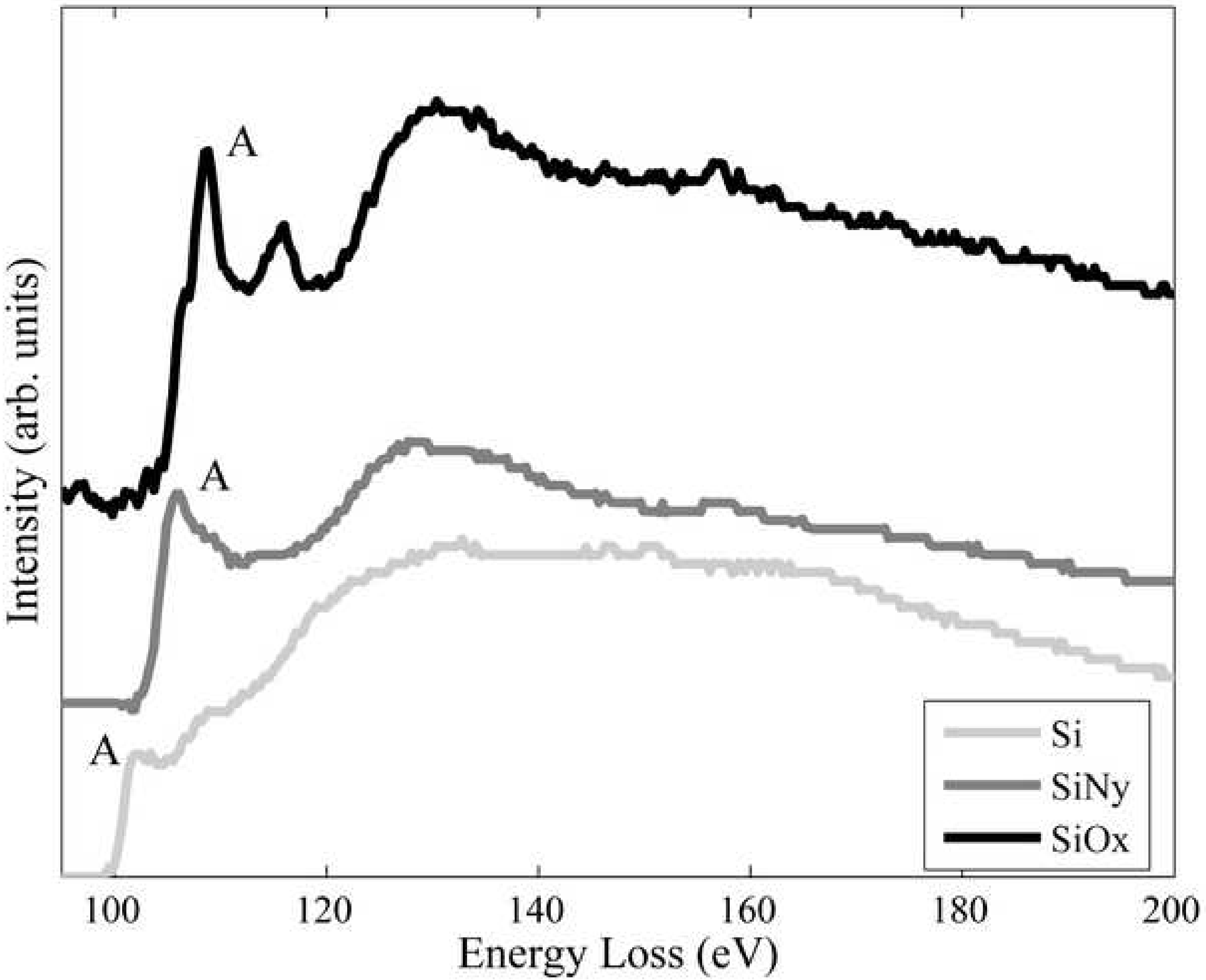
A
A
A
Intensity (arb. units)
100
120
140
160
180
200
Energy Loss (eV)
Si
SiNy
SiOx

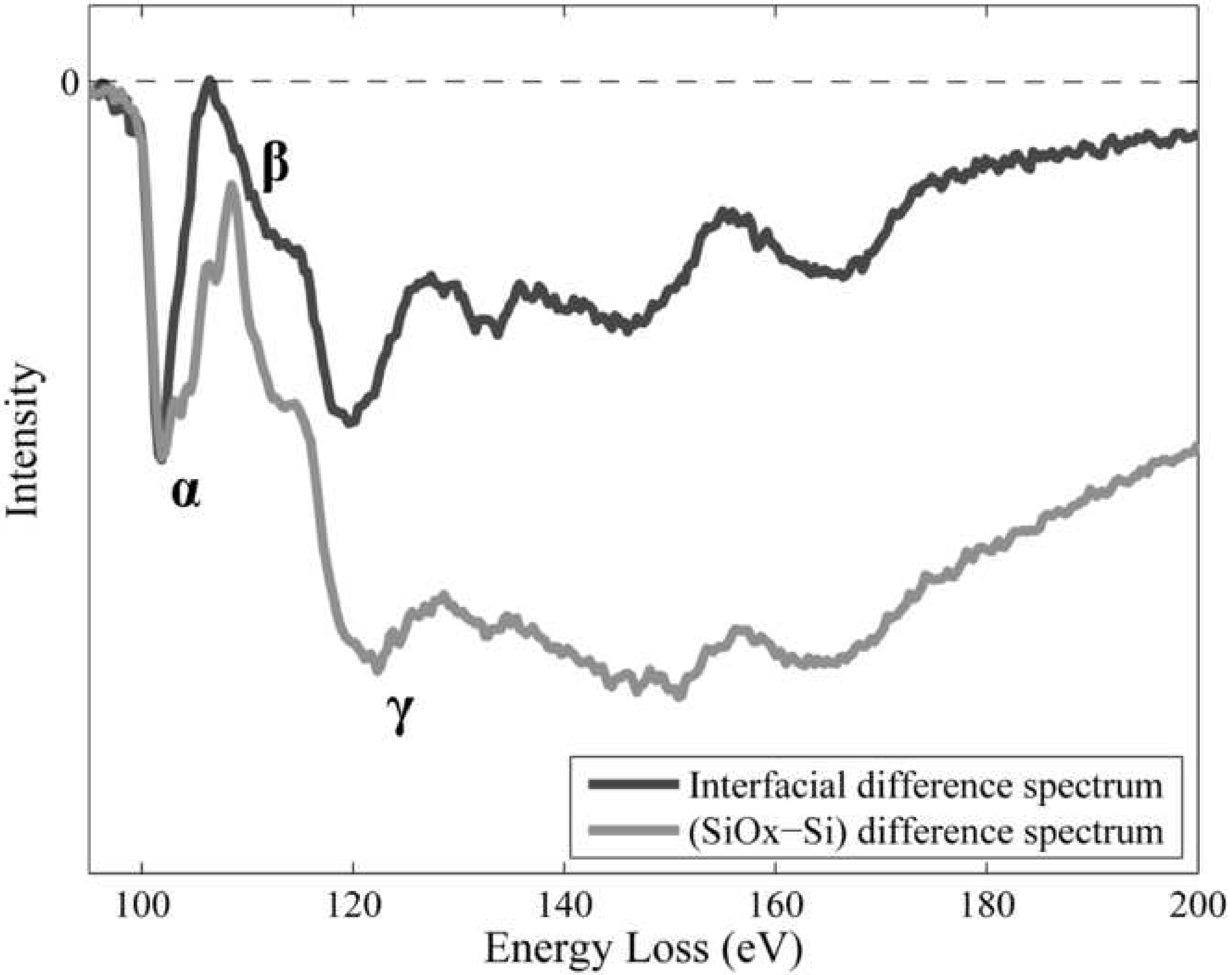
0
β
α
γ
Intensity
Interfacial difference spectrum
(SiOx−Si) difference spectrum
100
120
140
160
180
200
Energy Loss (eV)

Figure

Click here to download high resolution image

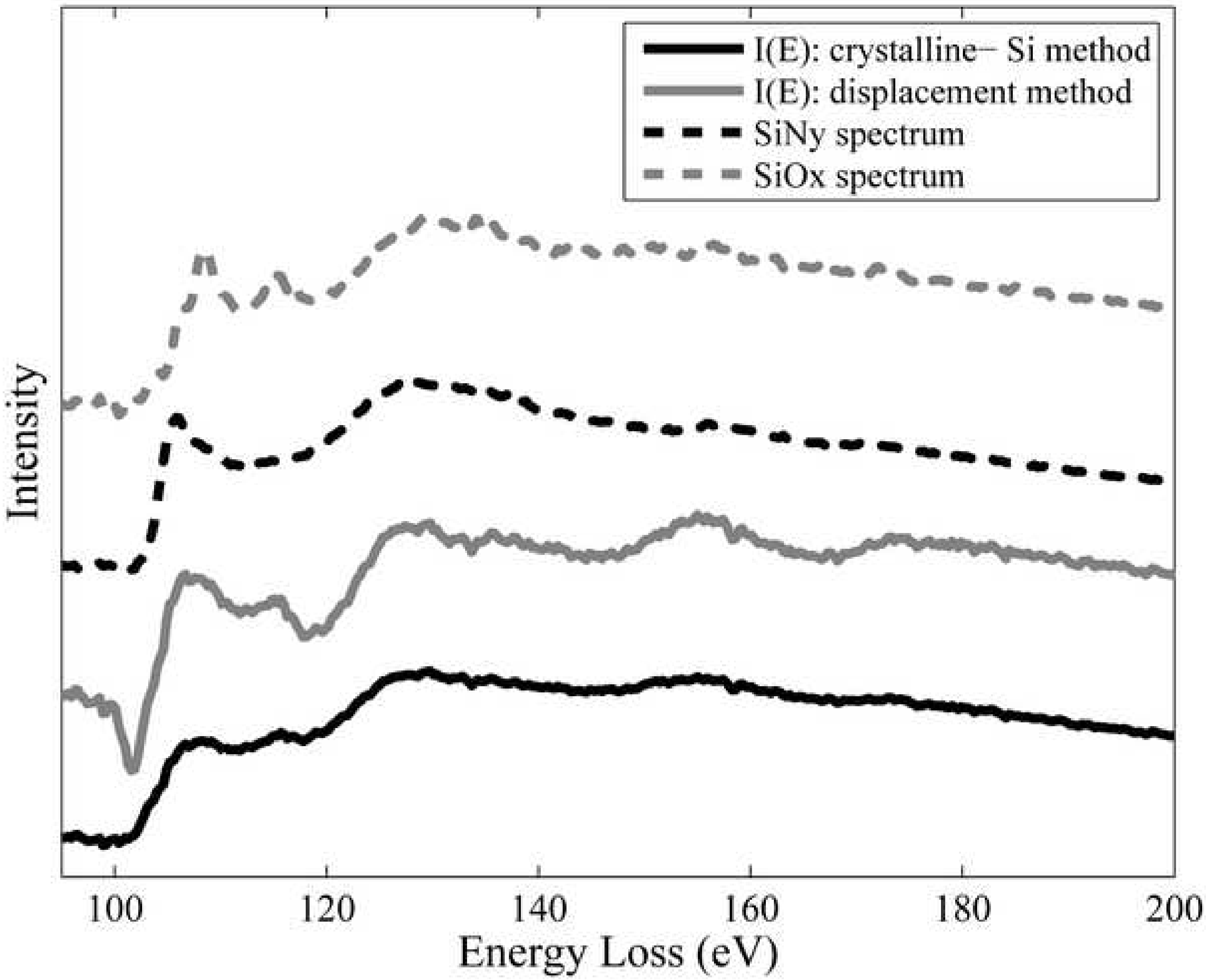

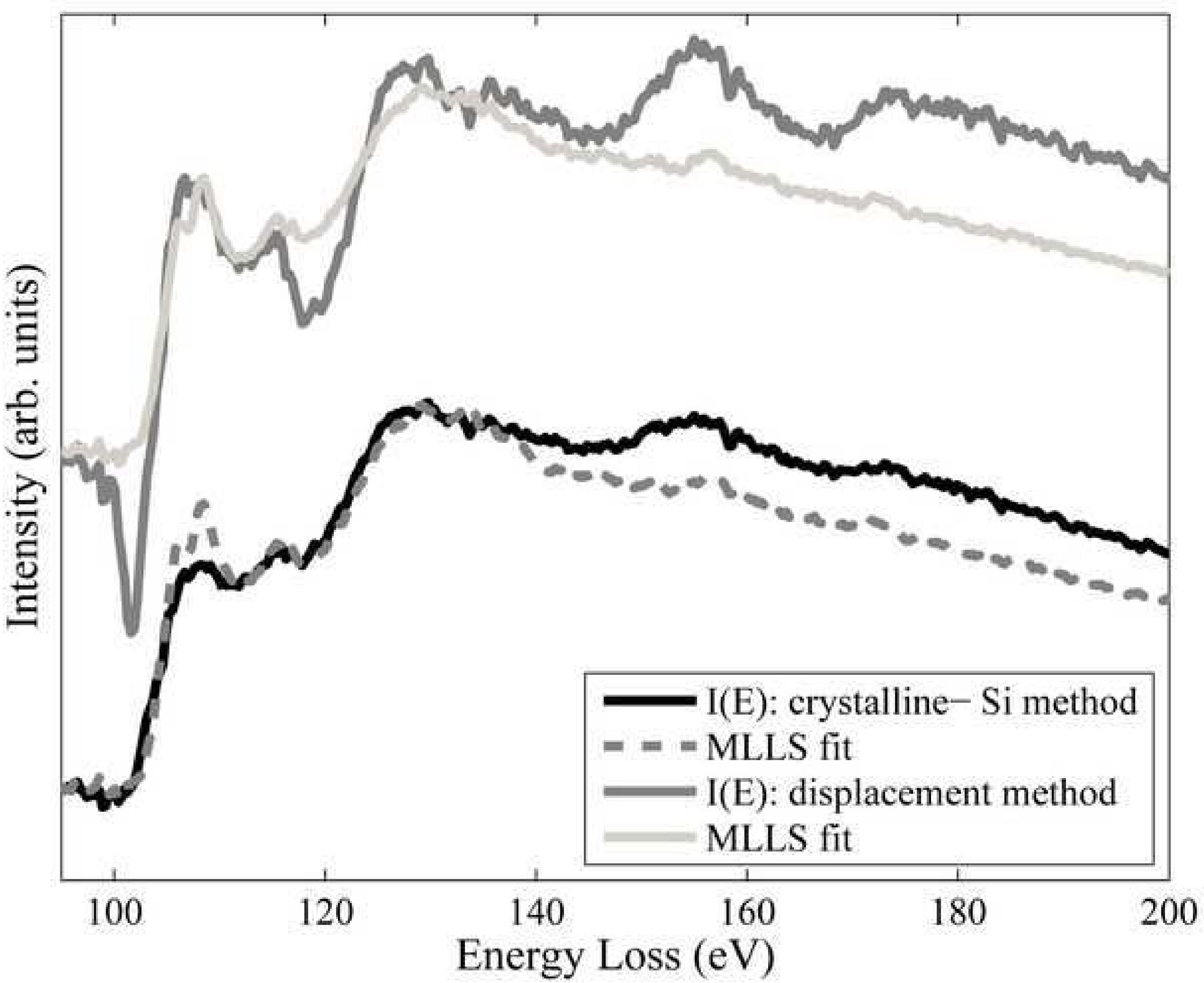
Intensity (arb. units)
100
120
140
160
180
200
Energy Loss (eV)
I(E): crystalline− Si method
MLLS fit
I(E): displacement method
MLLS fit

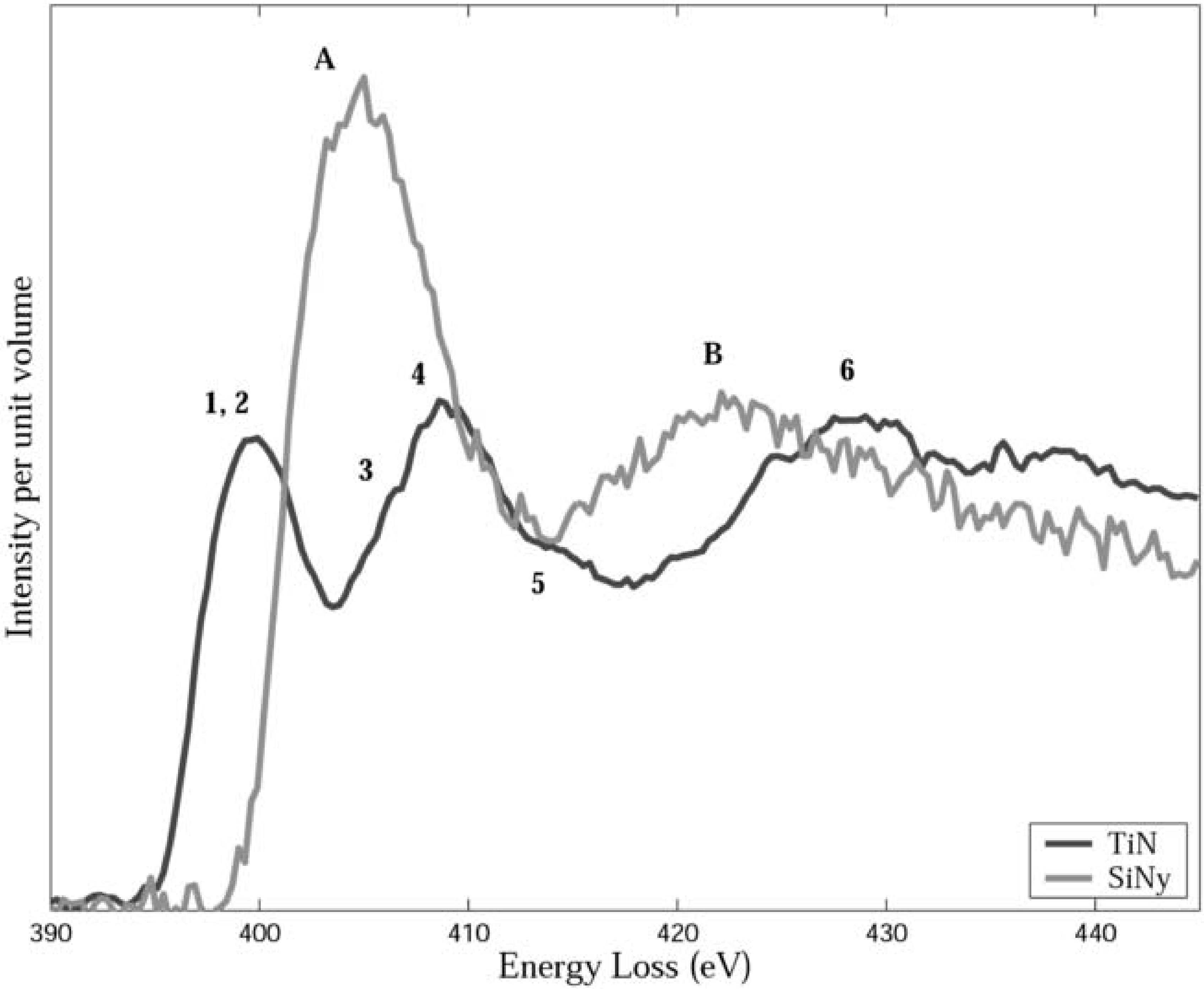
A
B
1, 2
3
4
5
6
TiN
SiNy
Intensity per unit volume
Energy Loss (eV)
390
400
410
420
430
440

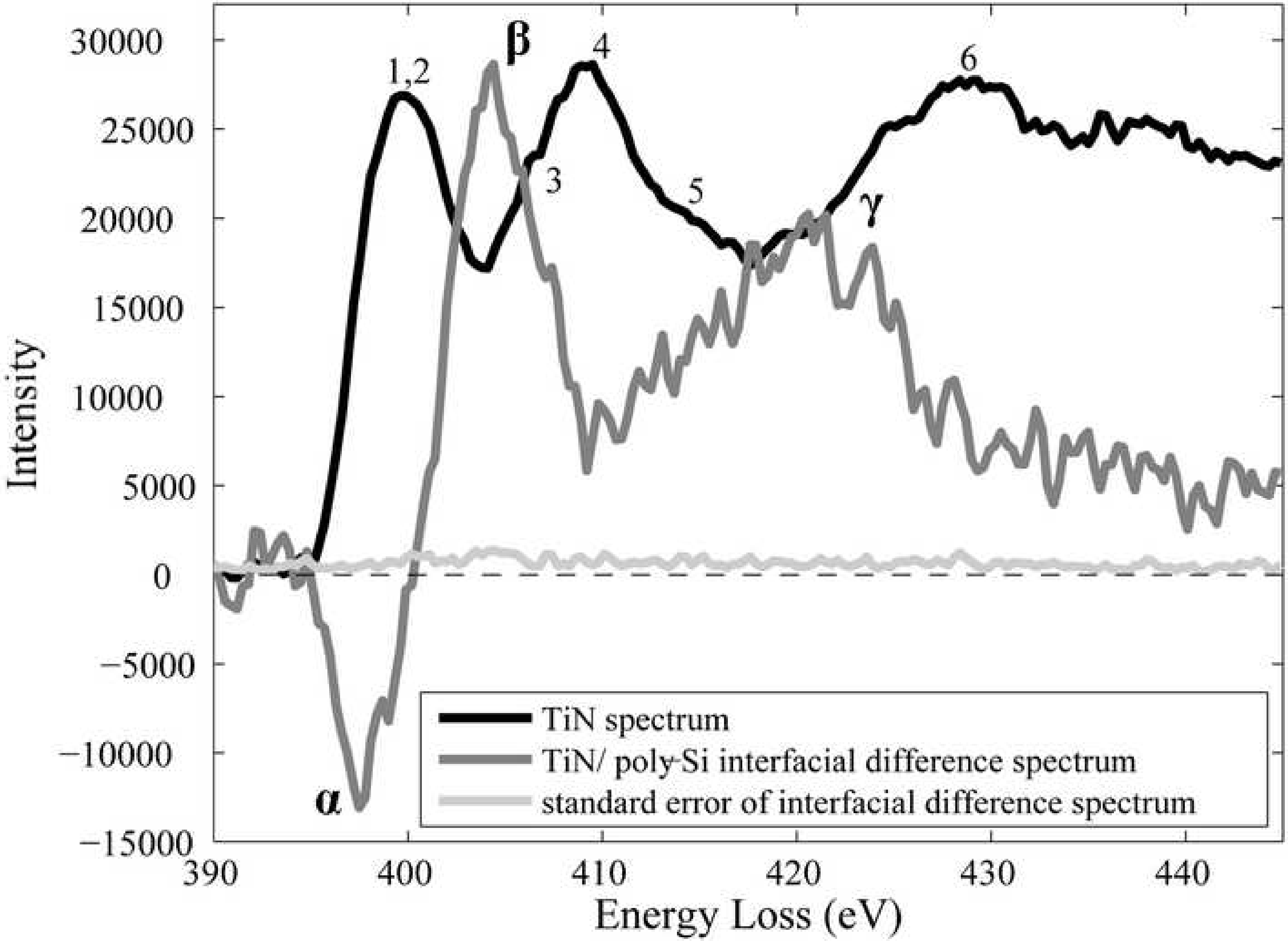
Intensity
30000
25000
20000
15000
10000
5000
0
−5000
−10000
−15000
390
400
410
420
430
440
Energy Loss (eV)
1,2
β
4
6
3
5
γ
α
TiN spectrum
TiN/ poly-Si interfacial difference spectrum
standard error of interfacial difference spectrum

Figure

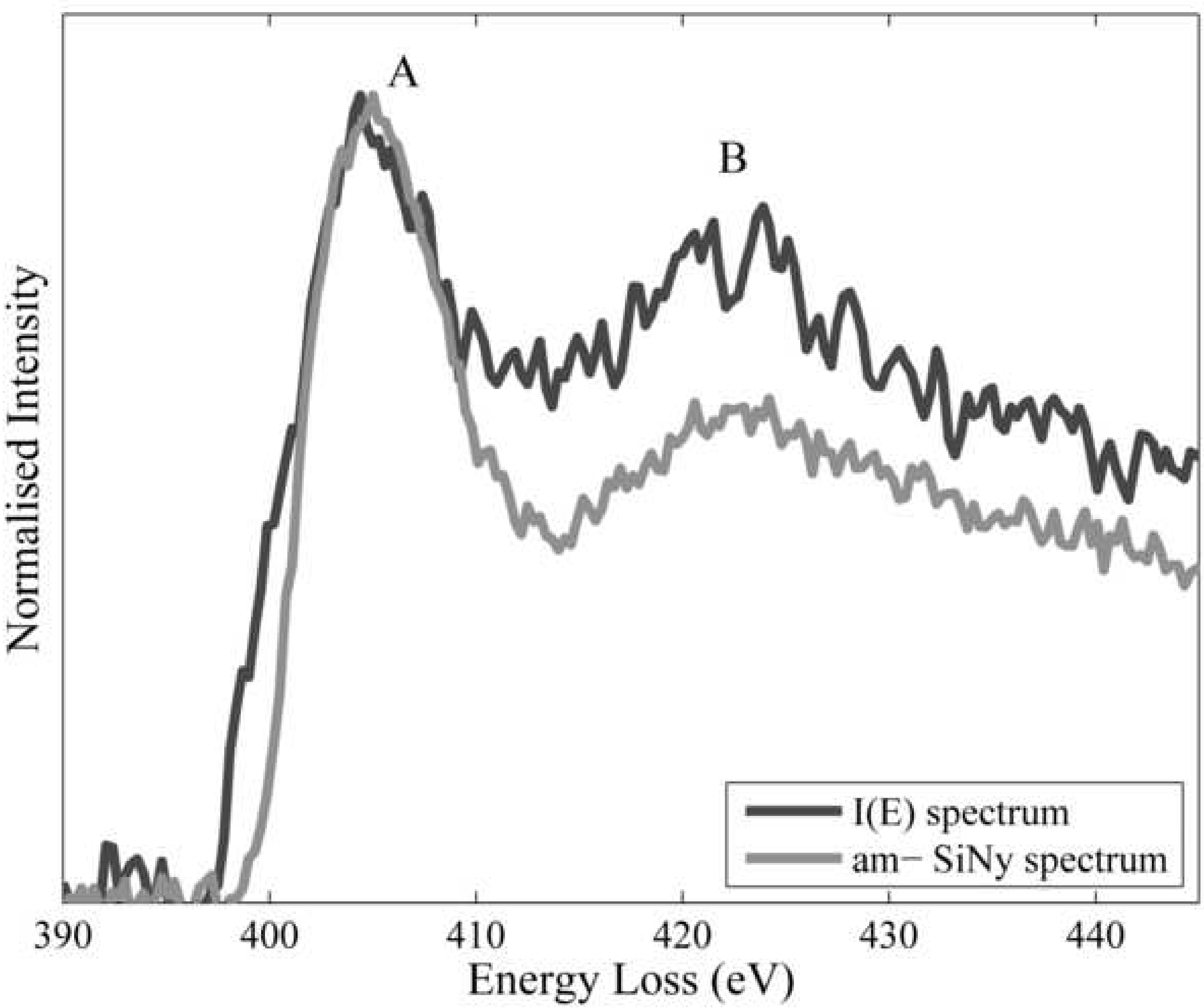
A
B
Normalised Intensity
390
400
410
420
430
440
Energy Loss (eV)
I(E) spectrum
am− SiNy spectrum

Figure

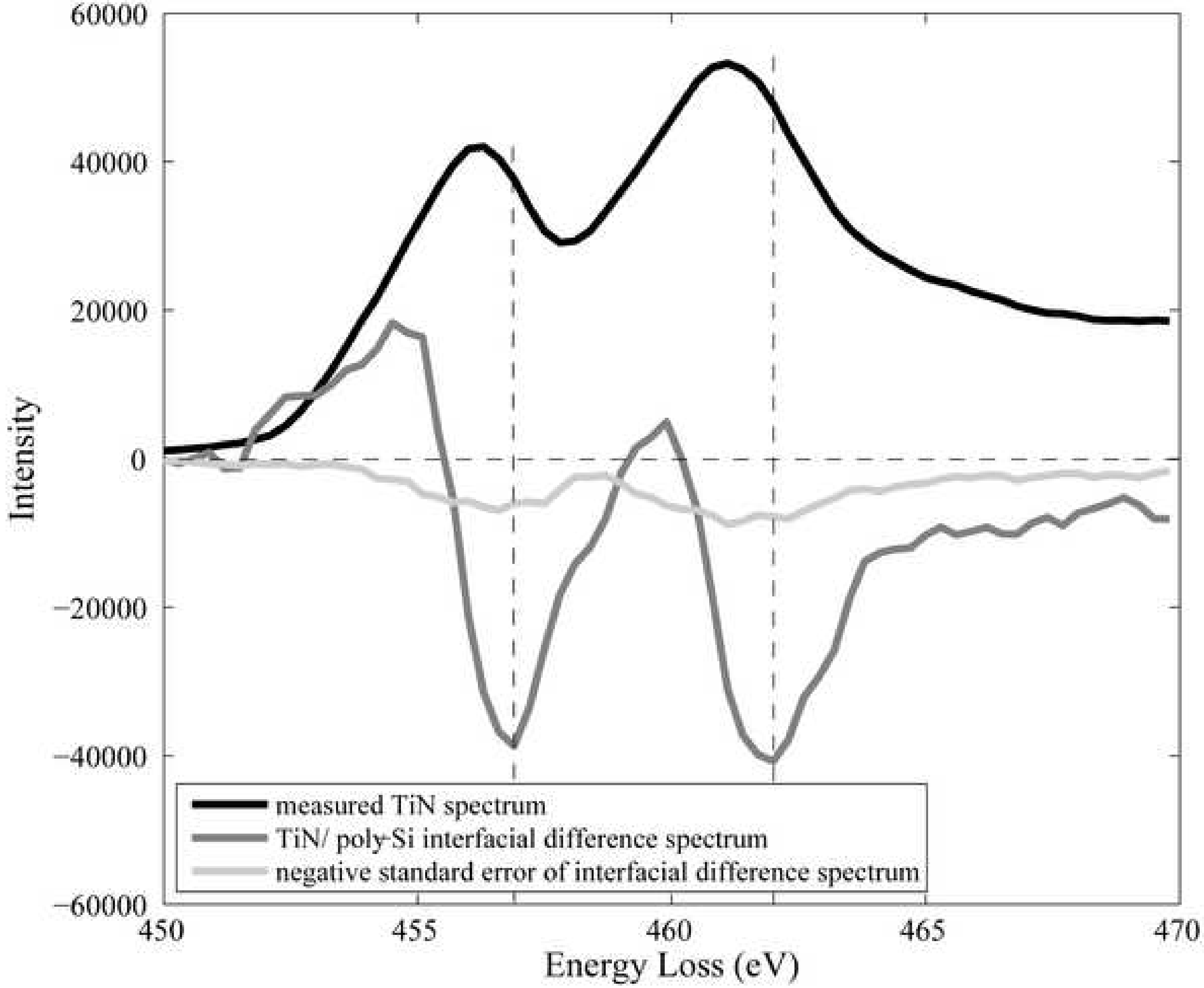
60000
40000
20000
0
−20000
−40000
−60000
Intensity
450
455
460
465
470
Energy Loss (eV)
measured TiN spectrum
TiN/ poly-Si interfacial difference spectrum
negative standard error of interfacial difference spectrum

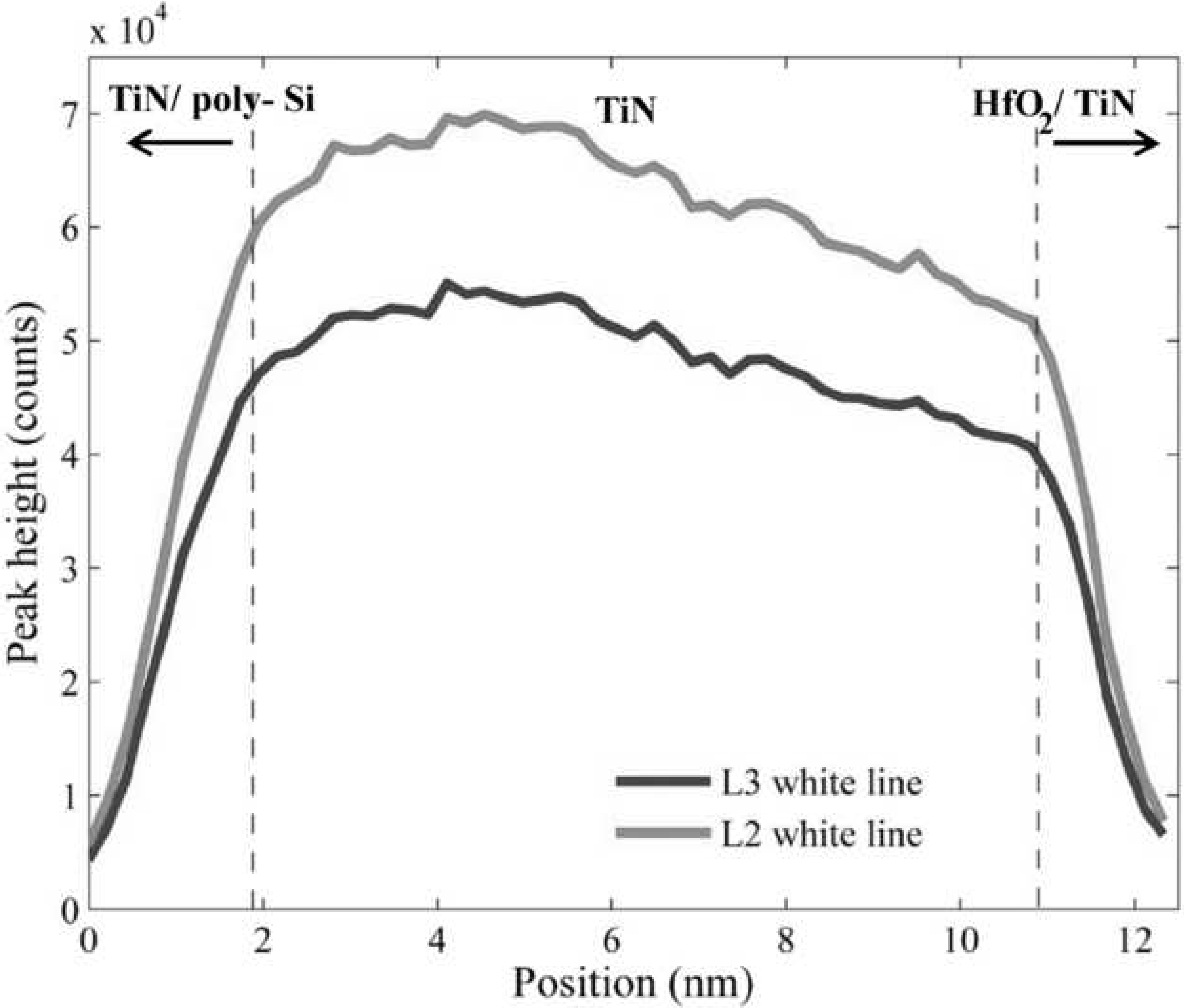
x 10^4
TiN/ poly- Si
TiN
HfO2/ TiN
Peak height (counts)
Position (nm)
0
1
2
3
4
5
6
7
0
2
4
6
8
10
12
L3 white line
L2 white line

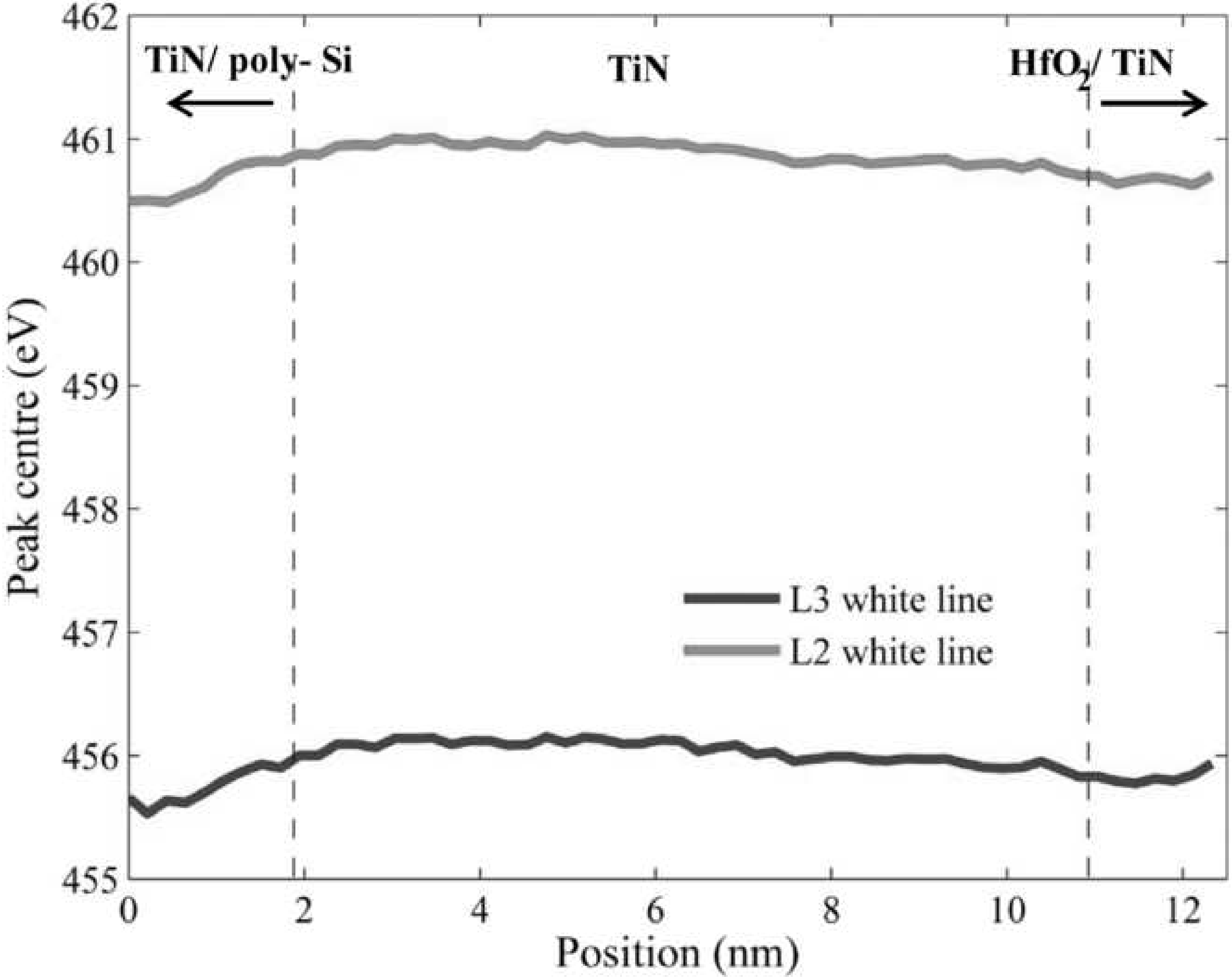
TiN/ poly- Si
TiN
HfO$_2$/ TiN
Peak centre (eV)
462
461
460
459
458
457
456
455
L3 white line
L2 white line
0
2
4
6
8
10
12
Position (nm)

Figure

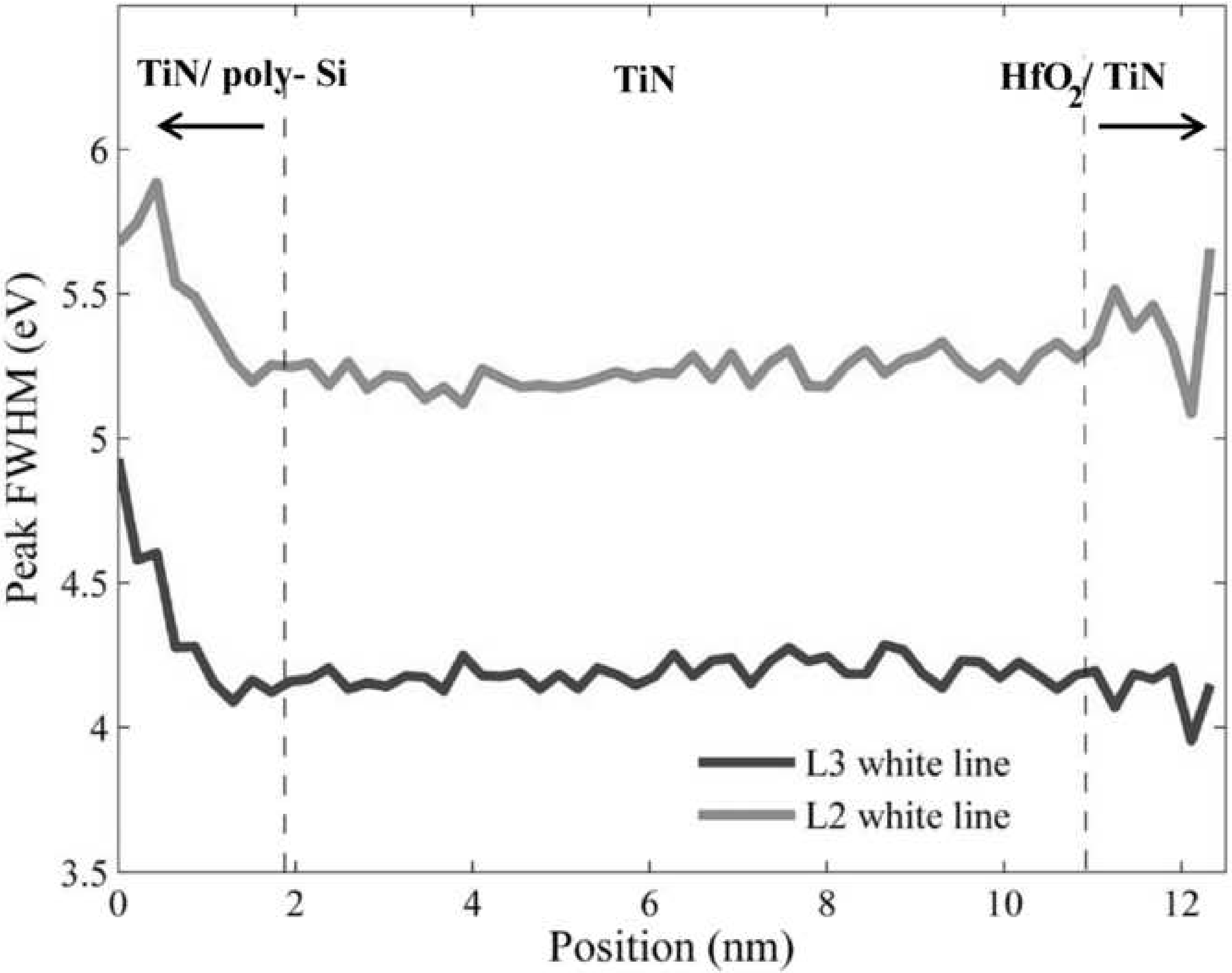
TiN/ poly- Si
TiN
HfO$_2$/ TiN
Peak FWHM (eV)
Position (nm)
L3 white line
L2 white line
6
5.5
5
4.5
4
3.5
0
2
4
6
8
10
12

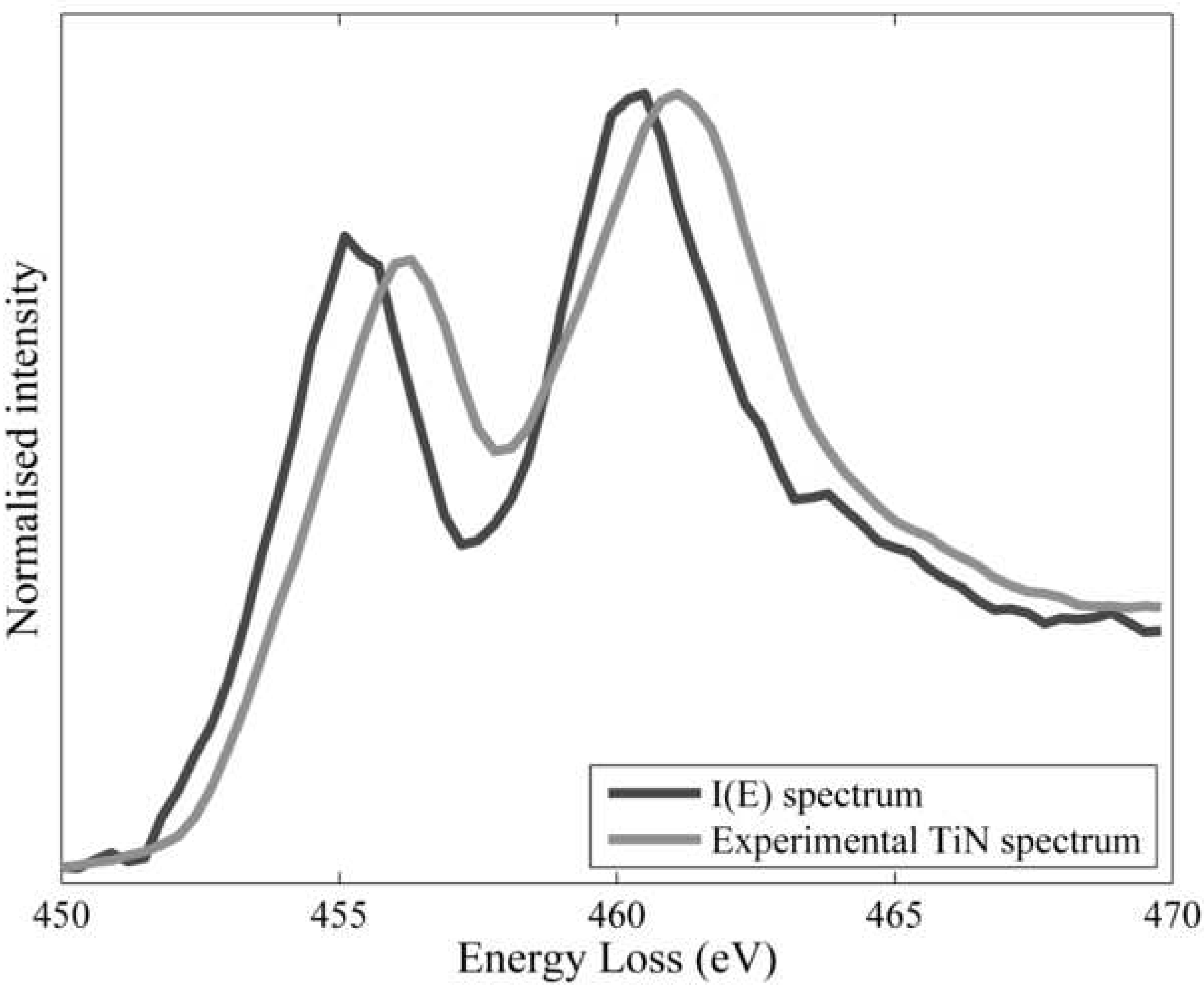
Normalised intensity
450
455
460
465
470
Energy Loss (eV)
I(E) spectrum
Experimental TiN spectrum

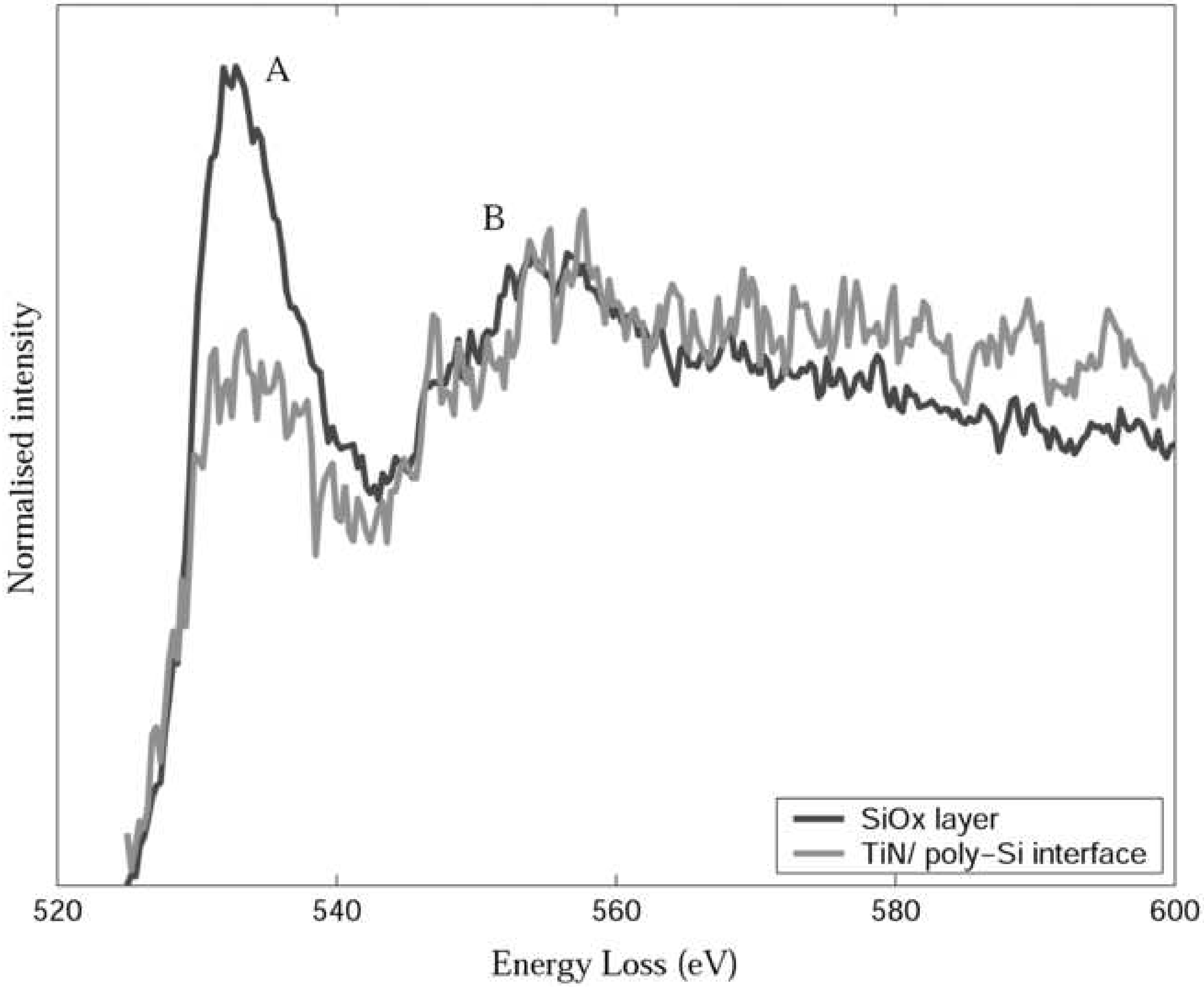
A
B
Normalised intensity
520
540
560
580
600
Energy Loss (eV)
SiOx layer
TiN/ poly−Si interface